

AD-A061 918

BATTELLE COLUMBUS LABS OHIO  
EARLY HEATING PROCESSES IN LASER-SUPPORTED DETONATION (LSD) WAV--ETC(U)  
OCT 78 C T WALTERS, A H CLAVER

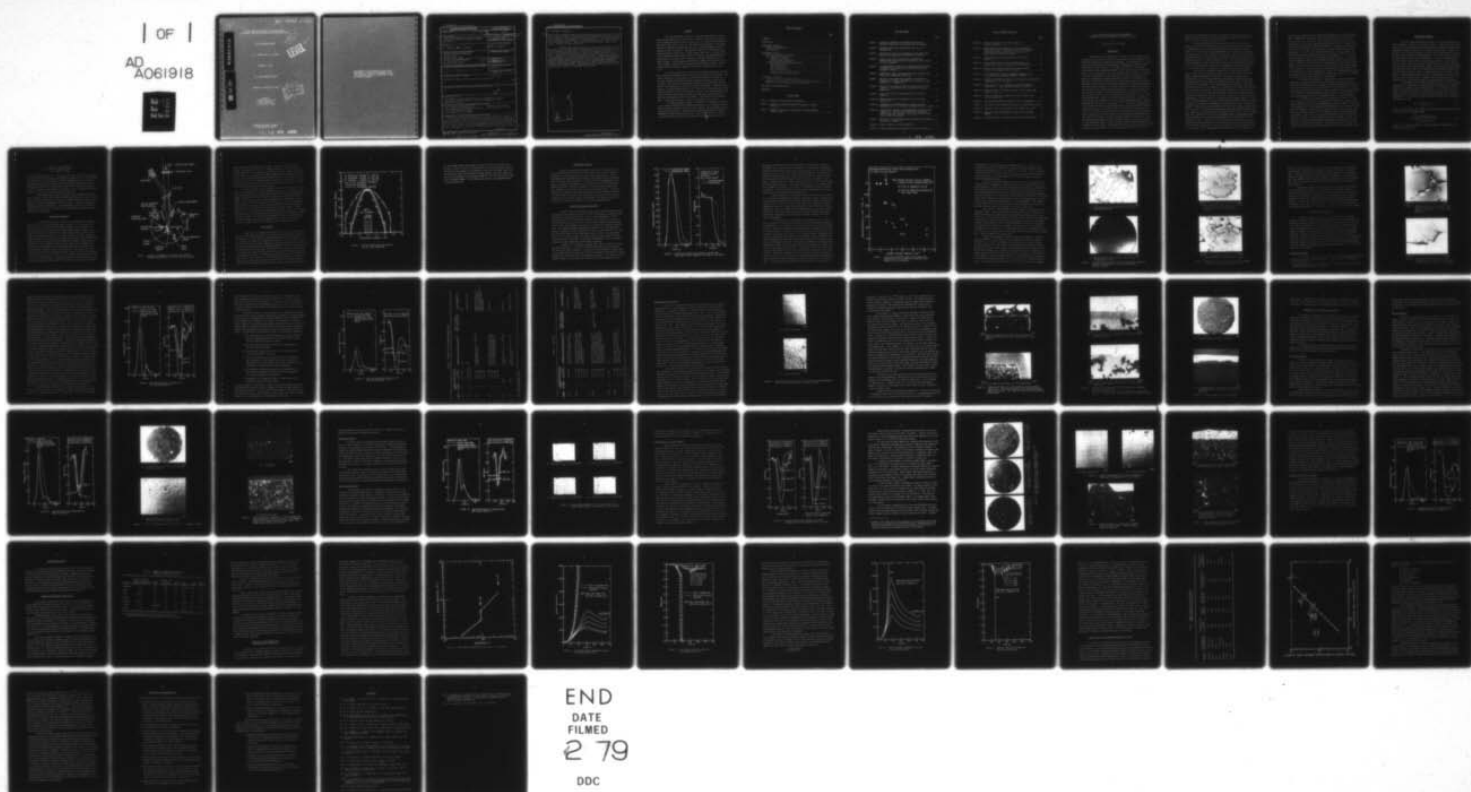
F/6 11/6  
DAAG29-76-C-0059

ARO-14045.2-MS

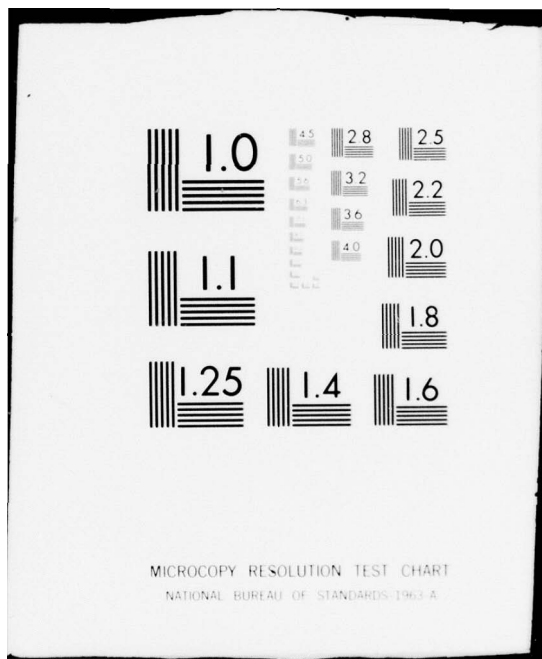
NL

UNCLASSIFIED

| OF |  
AD  
A061918  
SEE



END  
DATE  
FILMED  
2 79  
DDC



ARO 14045.2-MS

AD A061918

DDC FILE COPY

EARLY HEATING PROCESSES IN LASER-SUPPORTED  
DETONATION (LSD) WAVE INITIATION ON METALS AND ALLOYS

FINAL TECHNICAL REPORT

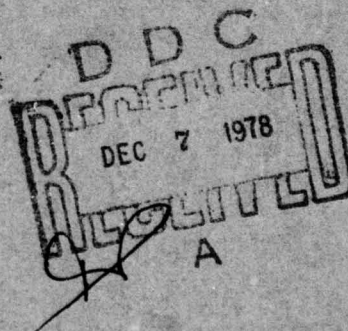
C. T. WALTERS and A. H. CLAUER

OCTOBER 15, 1978

U.S. ARMY RESEARCH OFFICE

CONTRACT NO. DAAG29-76-C-0059

BATTELLE  
Columbus Laboratories  
505 King Avenue  
Columbus, Ohio 43201



APPROVED FOR PUBLIC RELEASE;  
DISTRIBUTION UNLIMITED.

78 12 04 090

THE FINDINGS IN THIS REPORT ARE NOT TO BE  
CONSTRUED AS AN OFFICIAL DEPARTMENT OF THE  
ARMY POSITION, UNLESS SO DESIGNATED BY OTHER  
AUTHORIZED DOCUMENTS.

UNCLASSIFIED

SECURITY CLASSIFICATION OF THIS PAGE (When Data Entered)

DD FORM 1 JAN 73 1473 EDITION OF 1 NOV 65 IS OBSOLETE

UNCLASSIFIED

~~SECURITY CLASSIFICATION OF THIS PAGE (When Data Entered)~~

UNCLASSIFIED

SECURITY CLASSIFICATION OF THIS PAGE (When Data Entered)

20. Abstract (Continued)

tivity of metal samples subjected to intense TEA CO<sub>2</sub> laser radiation (50-100 ns pulse width) in a vacuum. The experimental configuration was selected to give a high degree of beam homogeneity on the sample surface. Metallographic examination of samples was performed to correlate changes in the surface structure with reflectivity results. Metals studied included aluminum, copper, iron, nickel, titanium, Al 2024, and Ti-6-4.

The data obtained were the first of their kind recorded at 10.6  $\mu$ m and revealed an anomalous effect in the specular reflectivity transient. The effect consisted of a sharp drop in reflectivity midway in the pulse to a low value (5-40%) followed by recovery to nearly the initial value late in the pulse. The effect was studied most extensively with aluminum, but was found to occur generally in the other materials irradiated. Considerable differences in thresholds and details of the effect were found which were attributable to materials effects and alloying. In most cases, metallographic examination revealed characteristic damage associated with samples which had exhibited the anomalous reflectivity effect. Implications of the anomalous effect for heating processes in metals are discussed in the report.

micrometers



UNCLASSIFIED

SECURITY CLASSIFICATION OF THIS PAGE (When Data Entered)

## FOREWORD

This report presents results of a two-year experimental study of early heating processes on metal and alloy surfaces under pulsed laser irradiation conditions which are known to give rise to so-called laser-supported detonation (LSD) waves at  $10.6 \mu\text{m}$ . The results are applicable to the understanding of LSD-wave initiation as well as to the understanding of pulsed heating of metals in general. The approach consisted of studying the time-resolved specular reflectivity of metal samples subjected to intense TEA  $\text{CO}_2$  laser radiation (50-100 ns pulse width) in a vacuum. The experimental configuration was selected to give a high degree of beam homogeneity on the sample surface. Metallographic examination of samples was performed to correlate changes in the surface structure with reflectivity results. Metals studied included aluminum, copper, iron, nickel, titanium, Al 2024, and Ti-6-4.

The data obtained were the first of their kind recorded at  $10.6 \mu\text{m}$  and revealed an anomalous effect in the specular reflectivity transient. The effect consisted of a sharp drop in reflectivity midway in the pulse to a low value (5-40%) followed by recovery to nearly the initial value late in the pulse. The effect was studied most extensively with aluminum, but was found to occur generally in the other materials irradiated. Considerable differences in thresholds and details of the effect were found which were attributable to materials effects and alloying. In most cases metallographic examination revealed characteristic damage associated with samples which had exhibited the anomalous reflectivity effect. Implications of the anomalous effect for heating processes in metals are discussed in the report.

The authors thank Mr. Warren B. Nicholson for technical assistance in the laser irradiations and Nomarski microscopy, Mr. Lee Dillinger for producing the taper sections, and Mr. George A. Wheeler for performing the scanning electron microscopy. The authors also thank Dr. Raymond W. Conrad of MIRADCOM for helpful discussions and Drs. George Mayer and John C. Hurt of the Army Research Office for their support and encouragement in this work.

TABLE OF CONTENTS

	<u>Page</u>
FOREWORD. . . . .	i
INTRODUCTION. . . . .	1
EXPERIMENTAL APPROACH . . . . .	4
Experimental Apparatus . . . . .	5
Beam Diagnosis . . . . .	7
EXPERIMENTAL RESULTS. . . . .	10
Thin-Film Aluminum Irradiations. . . . .	10
Bulk Aluminum Irradiations . . . . .	17
Reflectivity Results. . . . .	17
Metallographic Examination. . . . .	25
Irradiations of Other Metals and Alloys. . . . .	31
Pure Copper Results . . . . .	31
Pure Iron Results . . . . .	32
Pure Nickel Results . . . . .	36
Pure Titanium Results . . . . .	36
Aluminum Alloy (Al 2024) Results. . . . .	39
Titanium Alloy (Ti-6-4) Results . . . . .	45
DISCUSSION OF RESULTS . . . . .	47
Summary of Experimental Observations . . . . .	47
Comparison of Experimental Data with Theoretical Predictions . . . . .	49
Implications of the Anomalous Reflectivity Result. . . . .	57
CONCLUSIONS AND RECOMMENDATIONS . . . . .	62
REFERENCES. . . . .	64

LIST OF TABLES

TABLE 1. SUMMARY OF BULK ALUMINUM IRRADIATIONS . . . . .	23
TABLE 2. SUMMARY OF ANOMALOUS REFLECTIVITY BEHAVIOR IN METALS AND ALLOYS. . . . .	48
TABLE 3. PROPERTY DATA USED IN CALCULATION OF DAMAGE THRESHOLD FIGURE OF MERIT . . . . .	58

LIST OF FIGURES

	<u>Page</u>
FIGURE 1. SCHEMATIC ARRANGEMENT OF APPARATUS FOR MEASURING TRANSIENT REFLECTIVITY OF BULK AND THIN-FILM SAMPLES . . . . .	6
FIGURE 2. MEASURED TARGET PLANE BEAM PROFILES FOR CO <sub>2</sub> LASER IRRADIATIONS . . . . .	8
FIGURE 3. REFLECTIVITY RESULTS FOR ALUMINUM FILM WITH PEAK POWER DENSITY ABOVE THRESHOLD FOR COMPLETE FILM REMOVAL . . . . .	11
FIGURE 4. TIMING OF REFLECTIVITY CUTOFF FOR ALUMINUM FILM IRRADIATIONS (DATA ADJUSTED FOR EQUIVALENT ENERGY DENSITY AT 120 nm THICKNESS) . . . . .	13
FIGURE 5. LOW MAGNIFICATION VIEWS OF THE LASER-IRRADIATED SURFACES OF ALUMINUM FILMS DEPOSITED ON POLISHED FUSED QUARTZ (NOMARSKI LIGHTING) . . . . .	15
FIGURE 6. APPEARANCE OF SMALL RUPTURED AREAS IN THE ALUMINUM FILM AFTER LASER IRRADIATION, SAMPLE QA-5. . . . .	16
FIGURE 7. REGION OF LASER-IRRADIATED ALUMINUM FILM SHOWING THE FORMATION OF BLISTERS, RUPTURING OF A BLISTER AT A, AND MELTING AT B. SAMPLES QA-5 . . . . .	18
FIGURE 8. MELTING OF THE ROLLED-UP EDGE OF THE ALUMINUM FILM AND THROWING OF THE DROPLETS IN THE DIRECTION OF ROLLING. SAMPLE QA-5 . . . . .	18
FIGURE 9. SPECULAR REFLECTIVITY TRANSIENTS FOR BULK ALUMINUM SAMPLE A-4. . . . .	20
FIGURE 10. SPECULAR REFLECTIVITY TRANSIENTS FOR BULK ALUMINUM SAMPLE A-8(b) . . . . .	22
FIGURE 11. APPEARANCE OF ALUMINUM SAMPLE A-5 BEFORE AND AFTER IRRADIATION AT $3.1 \times 10^8$ W/cm <sup>2</sup> PEAK POWER DENSITY (1 PULSE) .	26
FIGURE 12. TAPER SECTION THROUGH A LASER-IRRADIATED ALUMINUM SURFACE (SAMPLE A-8). THE SECTION INTERSECTS THE IRRADIATED SURFACE ALONG THE FLAT EDGE. THE SAMPLE WAS PLATED WITH NICKEL BEFORE METALLOGRAPHY . . . . .	28
FIGURE 13. PROFILES OF THE IRRADIATED SURFACE SHOWING GRAIN BOUNDARIES AND POROSITY (SAMPLE A-8) . . . . .	29
FIGURE 14. VIEWS OF SAMPLE A-9 AFTER IRRADIATION . . . . .	30
FIGURE 15. SPECULAR REFLECTIVITY TRANSIENTS FOR BULK IRON SAMPLE F-1 . .	33

LIST OF FIGURES (Continued)

	<u>Page</u>
FIGURE 16. VIEWS OF IRRADIATED IRON SURFACE SAMPLE F-1. (NOMARSKI LIGHTING) . . . . .	34
FIGURE 17. TAPER SECTIONS AT A NOMINALLY 10:1 TAPER THROUGH THE IRRADIATED SURFACE OF THE IRON SAMPLE. THE SAMPLE WAS NICKEL PLATED BEFORE SECTIONING AS INDICATED. THE ARROWS POINT TO PROFILES OF CRATERS . . . . .	35
FIGURE 18. SPECULAR REFLECTIVITY TRANSIENTS FOR BULK NICKEL SAMPLE N-3. . . . .	37
FIGURE 19. OSCILLOSCOPE RECORDS FOR BULK TITANIUM SAMPLE (T-1) SHOWING SHARP CUTOFF OF REFLECTIVITY WITH RECOVERY. . . . .	38
FIGURE 20. SPECULAR REFLECTIVITY TRANSIENTS FOR BULK ALUMINUM ALLOYS (2024) SAMPLES AA20-1 and AA20-2 . . . . .	40
FIGURE 21. LOW MAGNIFICATION VIEWS OF IRRADIATED SURFACES OF THE 2024 ALUMINUM ALLOY SAMPLES (NOMARSKI LIGHTING) . . . . .	42
FIGURE 22. NOMARSKI MICROGRAPHS OF SAME AREA OF SURFACE OF SAMPLE AA20-3 (SUBJECTED TO $2.3 \times 10^8$ W/cm <sup>2</sup> ) . . . . .	43
FIGURE 23. TAPER SECTION AT 10:1 THROUGH THE IRRADIATED SURFACE OF SAMPLE AA20-1. ARROW INDICATES BLOWN OUT INCLUSION . . . . .	43
FIGURE 24. TAPER SECTION OF THE SAMPLE SUBJECTED TO THE HIGHEST BEAM INTENSITY (AA20-2) . . . . .	44
FIGURE 25. SPECULAR REFLECTIVITY TRANSIENT FOR BULK TITANIUM ALLOY (Ti-6-4) SAMPLE T64-1 . . . . .	46
FIGURE 26. PURE ALUMINUM ABSORPTIVITY MODEL AT 10.6 $\mu$ m WAVELENGTH. . . . .	51
FIGURE 27. PREDICTED SURFACE TEMPERATURE HISTORY FOR ALUMINUM THIN FILM. 52	52
FIGURE 28. PREDICTED REFLECTIVITY TRANSIENT FOR ALUMINUM THIN FILM . . . . .	53
FIGURE 29. PREDICTED SURFACE TEMPERATURE HISTORY OF BULK ALUMINUM SAMPLE. . . . .	55
FIGURE 30. PREDICTED REFLECTIVITY TRANSIENT FOR BULK ALUMINUM SAMPLE . . . . .	56

EARLY HEATING PROCESSES IN LASER-SUPPORTED  
DETONATION (LSD) WAVE INITIATION ON METALS AND ALLOYS

by

C. T. Walters and A. H. Clauer

INTRODUCTION

When pulsed laser radiation is incident on a solid surface in air, a plasma may be initiated in the air at the surface for power densities well below those required for ordinary air breakdown. The hot plasma ( $T_e \approx 1-2$  eV) is almost totally absorbing and propagates at supersonic speed back up the laser beam for power densities in the range  $10^6$ - $10^9$  W/cm<sup>2</sup>. This laser-driven shock or laser-supported detonation (LSD) wave completely alters the nature of the interaction of the laser radiation with the target. Generally, for metals in the absence of the LSD wave, the mechanical response of the material is dominated by vaporization effects, while in the presence of LSD waves, the pressures caused by the air blast-wave dominate the response. Furthermore, the presence of an LSD-wave plasma can increase or decrease the effective thermal coupling of the laser radiation to the material depending upon the laser pulse shape and peak power density. For these reasons, LSD-waves became the subject of intense investigation in recent years. While most research efforts to date on LSD waves have been devoted to study of the LSD waves and their effects after they have been initiated, a two-year research program was conducted at Battelle under DARPA sponsorship to isolate mechanisms of initiation of these waves.<sup>(1,2,3)</sup> The primary conclusion from this research was that the experimental data on practical aluminum surfaces irradiated with 10.6- $\mu$ m TEA laser pulses (with peak power density greater than  $5 \times 10^7$  W/cm<sup>2</sup>) are consistent with an initiation model, wherein surface-emitted priming electrons are heated by inverse-bremsstrahlung absorption in the field of the neutral air molecules which results in initiation of a non-equilibrium air-breakdown cascade. Thermionic emission (or field emission at high peak-power density) at preferentially heated surface features such as lamination and pit defects is believed to be the process of free-electron production at a large number of local initiation sites ( $\sim 10^4$  cm<sup>-2</sup>). The

individual LSD plasmas are believed to "link up" as they move away from the surface and spread laterally. At lower peak-power densities, breakdown in the metal vapor is believed to play a role.<sup>(4)</sup>

It became apparent in the LSD-wave initiation research that the details of the early heating processes on the metal surface were critical to an understanding of the initiation process which is apparently thermally driven.<sup>(1)</sup> In particular, the optical absorptivity of metals as a function of temperature is not well understood and unusually high values of absorptivity were required to force agreement of results of simple heating theory with experimental values of LSD-wave initiation time. The research reported herein was undertaken to obtain basic data on the optical absorptivity of metals at 10.6  $\mu\text{m}$  which would be relevant to the LSD-wave initiation problem as well as to the general area of interaction of intense laser beams with metals.

Some previous research on absorption of intense laser pulses on metal surfaces has been conducted, however, most of this work has been performed at short wavelengths ( $\leq 1.06\text{-}\mu\text{m}$ ). The earliest work was that of Bonch-Bruevich et al.<sup>(5)</sup> who examined the time-resolved reflectivity during individual spikes (500 ns FWHM) of a normal mode 1.06  $\mu\text{m}$  laser pulse interacting with metal surfaces in an integrating sphere arrangement. The laser beam intensity profile was claimed to be uniform, but the target plane profile was not discussed explicitly. The temperature dependence of the optical absorptivity was extracted from the reflectivity data and heat-transfer analyses. A jump in the absorptivity of silver at 1.06  $\mu\text{m}$  (from .25 to .60) was found to correspond to the melt transition. Peak power density was reported as  $6 \times 10^7$  W/cm<sup>2</sup>. Similar experiments were reported by Chun and Rose,<sup>(6)</sup> however, no attempt to extract the temperature dependence of absorptivity was made. Levinson and Smilga<sup>(7)</sup> studied the optical reflectance of thin films of noble metals irradiated at 337 nm. The reflectance measurements were made during the laser pulse (8 ns FWHM) with a continuous He-Ne laser probe beam (632 nm). While the experiments were carried out below the melt temperature only, a temperature-dependent absorptance was observed and correlated with the Drude theory for this temperature range. Zavecz et al.<sup>(8)</sup> recently performed irradiations of bulk copper and tantalum samples with 1.06- $\mu\text{m}$  Q-switched pulses (60 ns FWHM) wherein they measured reflectance of the laser-radiation within the specular cone for conditions yielding temperatures below and above the melt transition.

Below the melt transition, their data for reflectance as a function of time show a reproducible, anomalously low plateau with recovery to full reflectivity at the end of the pulse. Above the melt threshold, their results are similar to the results obtained by Bonch-Bruevich et al.; however, they attribute their additional drop in reflectance to formation of a dielectric-like layer in the molten zone rather than a change in absorptance at high temperature. This theory was invoked by Batanov et al.<sup>(9)</sup> to explain the Bonch-Bruevich results, although not without disagreement.<sup>(10,11)</sup> It should be noted that the laser pulse investigated by Bonch-Bruevich et al. was an order or magnitude longer than the Q-switched pulse and more time was available to establish an ablation wave<sup>(12)</sup> and associated dielectric-like layer. Whether or not this effect occurs on a scale of several tens of nanoseconds is not understood. In more recent work by Bonch-Bruevich and Potapov,<sup>(13)</sup> the transition of a 30- $\mu\text{m}$  thick layer of mercury to a transmitting dielectric-like state has been observed directly for long 1.06- $\mu\text{m}$  pulses (1 ms) incident at intensities below that required for vaporization.

An alternate explanation for the initial reversible reflectivity transition to anomalously low values is provided by the work of Koo and Slusher<sup>(14)</sup> who postulated the existence of temporary grading-like structures on the surface which scatter the radiation out of the specular cone. Their large angle scattering measurements at 1.06  $\mu\text{m}$  confirm some transient increase in the diffuse reflectivity; however, this increase is at most a factor of three over background, which is exceedingly small for a mirror surface.

In summary, data taken at 1.06  $\mu\text{m}$  indicate that there is a transient decrease in reflectivity of metal surfaces subjected to intense pulses which is anomalously large and unexplainable by classical theory. The causes of the anomaly are not well understood, particularly for the short pulse case. Almost no transient reflectivity data exist for 10.6- $\mu\text{m}$  laser pulses. Some data were obtained by Ready<sup>(15)</sup> but temporal resolution of the measurement was limited to 100 ns, far too slow for observation of effects relevant to LSD-wave initiation. The data reported herein are believed to be the first results of fast-response measurements of transient reflectivity of metals subjected to intense 10.6- $\mu\text{m}$  pulses. Reflectivity data were obtained for both thin film and bulk pure metal targets and as well as bulk alloy targets.

EXPERIMENTAL APPROACH

The basic approach selected for study of the optical absorption of metals subjected to  $10.6-\mu\text{m}$  laser pulses follows, to some extent, the earlier work at shorter wavelengths in that reflectivity transients are measured and information regarding absorptivity is inferred from the data. A major difference in the current measurements, however, arises from attempts to insure that the reflected signal is representative of the reflectivity of material at substantially uniform surface temperature. It is not clear that that is the case in much of the prior work at short wavelengths. In the previous work, the target samples were always spot-loaded, i.e. the laser irradiance area was always much smaller than the target. This method will give meaningful reflectivity data only if the target plane energy density profile has a "top-hat" shape (constant inside of a given radius and zero outside of that radius) or elaborate precautions are taken to ensure that only the central portion of the irradiance area is imaged on the reflectivity detector. Obviously only the former method works for integrating sphere measurements.

As an example of the difficulty that can arise if the target plane irradiance is not uniform in the spot-loading case, consider the reflected signal from a gaussian profile irradiance area. If the reflected signal is simply collected and directed to a detector without imaging, it will be a spatial average over surface regions of widely differing power density and temperature. If the reflectivity were such that locally on the surface at some instant in time

$$R(r) = \begin{cases} 0 & \text{for } r < r_o \\ 1 & \text{for } r \geq r_o \end{cases}, \quad (1)$$

where  $r_o$  is the gaussian spot radius, then the measured reflectivity at that instant would be the spatial average

$$R_m = \frac{\int_{r_o}^{r^*} R(r) \exp(-r^2/r_o^2) r dr}{\int_{r_o}^{r^*} \exp(-r^2/r_o^2) r dr}, \quad (2)$$

where  $r^*$  is a truncation radius. Using the example of Equation(1), the measured reflectivity is

$$R_m = \frac{\left[ \exp(-1) - \exp(-r^*{}^2/r_o{}^2) \right]}{\left[ 1 - \exp(-r^*{}^2/r_o{}^2) \right]} \quad . \quad (3)$$

If the truncation radius is  $r^* = 2r_o$ ,  $R_m = 0.36$ , which conveys little information about the true reflectivity as indicated by Equation (1). As noted above, this difficulty can be avoided by carefully imaging the central portion of the irradiance area on the detector, but maintaining alignment may be quite difficult, particularly for small spot sizes, such as those used by Zavecz et al.<sup>(8)</sup> ( $\approx 20 \mu\text{m}$ ). Maintenance of alignment of such a system would be more difficult in the far infrared region of the spectrum.

In the present work, these difficulties were eliminated by employing a so-called "flood-loaded" target arrangement, wherein the target is much smaller than the beam focal spot and nearly uniform irradiance conditions are achieved. The main disadvantage of such a system is increased difficulty in sample preparation and handling. This disadvantage is offset by increased reliability of the data. The details of the experimental apparatus and procedure are outlined below.

#### Experimental Apparatus

The experimental apparatus used for all measurements of transient reflectivity is illustrated schematically in Figure 1. The  $10.6\text{-}\mu\text{m}$  laser beam was focused by a 105-cm focal length germanium lens and sampled by a KCl optical flat which served as the vacuum chamber entrance window. The window reflections were directed to a CILAS 17-mm aperture carbon cone calorimeter for diagnostic purposes. The target samples consisted typically of 0.16-cm diameter by 2.5-cm long polycrystalline elemental metal (0.99999 pure) rods having one end ground flat and mechanically polished. Samples were irradiated at a plane slightly behind the focal plane of the germanium lens. The target rod was arranged so that the polished surface was located in a fairly uniform irradiance region of the beam area. The sample was mounted so that it could pivot for alignment and was oriented such that the beam axis was incident on the flat end of the rod at an angle of approximately  $10^\circ$  relative to the surface normal. The specularly reflected beam was detected with a photon drag detector (Rofin Model 7410) mounted on a goniometer within the

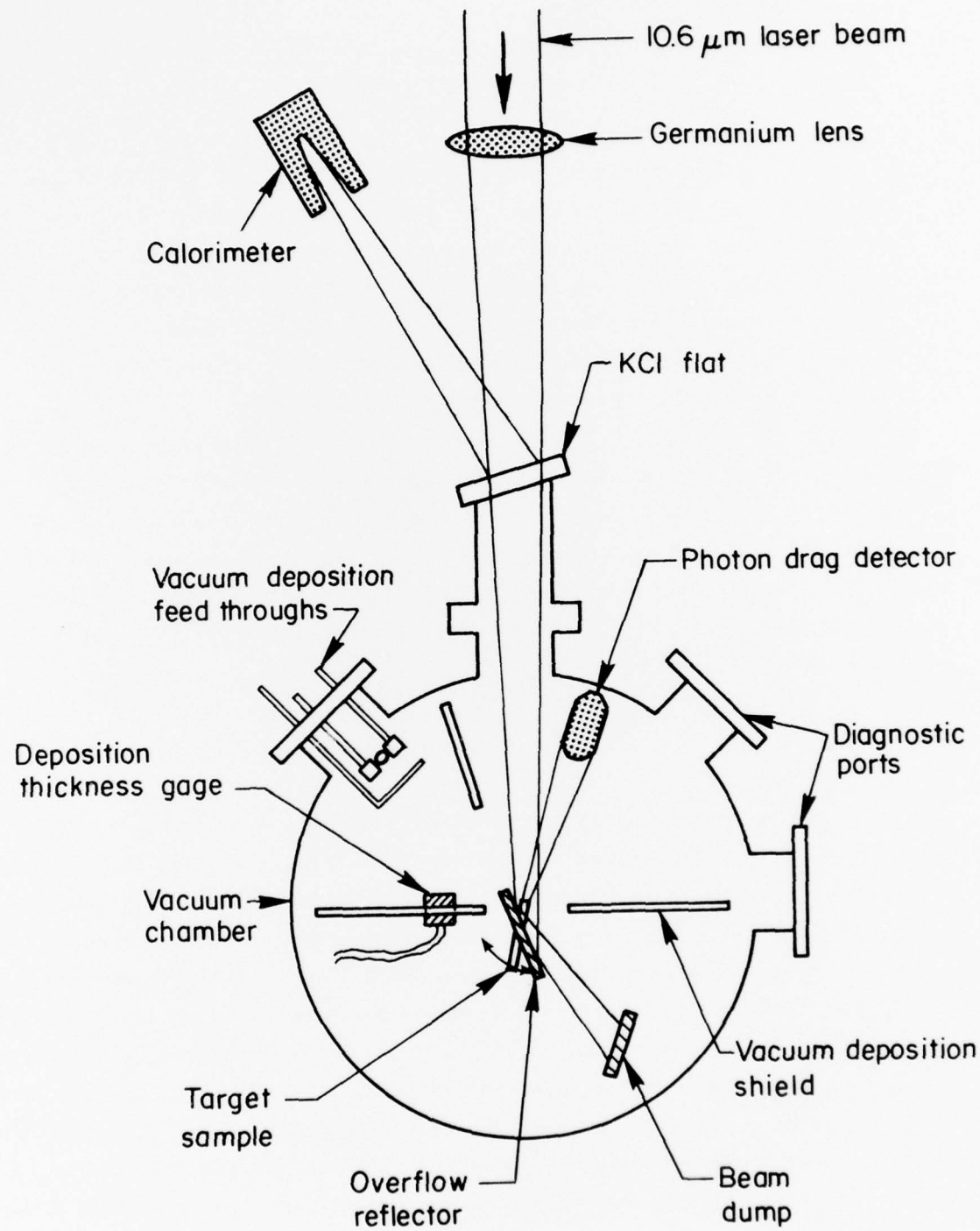


FIGURE 1. SCHEMATIC ARRANGEMENT OF APPARATUS FOR MEASURING TRANSIENT REFLECTIVITY OF BULK AND THIN-FILM SAMPLES

vacuum chamber as illustrated in the figure. The detector was connected through a terminated 50- $\Omega$  line to a 150-MHz bandwidth, 2.4-ns risetime oscilloscope (TEK-7704). The radiation overflowing the target sample was diverted by a reflector to a beam dump in a manner which precluded significant interference with the specularly reflected signal detection. The chamber was evacuated with a six-inch oil diffusion pump with cryogenic cold trap. Provisions for vapor deposition of metal films were arranged as indicated in the figure and included a quartz film thickness monitor.

The laser employed in the study was a Lumonics Model 301 which provides 75 J (multimode) in a normal TEA-laser pulse. For this research, the laser was operated without nitrogen gas in the laser mixture and the maximum energy was approximately 20 J in a gain-switched pulse of width 50-100 ns (FWHM). Beam energy was varied in the experiments by introduction of polyethylene and metal screen attenuators near the laser. For a fixed position within the focal spot area, shot-to-shot reproducibility of pulse shape was better than 5-10% depending on the portion of the pulse examined. Pulse shape did vary as a function of position within the focal spot and this limited the usefulness of a window reflection for monitoring the incident pulse shape for the rod sample. The incident pulse shape for each high intensity shot was inferred, therefore, from the reflected pulse shape from a previous low intensity irradiation where the reflectance did not change with time.

#### Beam Diagnosis

Since the laser employed was a multimode laser, the irradiance profile at various target positions in the beam was not predictable from theory. To determine the target surface energy density and degree of homogeneity, it was necessary to measure the energy density profile. This was done using a previously developed technique employing calibrated attenuators and a material at the target plane having a well-defined damage threshold, cellulose acetate.<sup>(3)</sup> Iso-energy-density contours were constructed from a sequence of irradiations of varying total energy and these contours were measured to provide profiles as illustrated in Figure 2. Profiles are given for two positions behind the focal plane at which two series of reflectivity experiments were conducted. Also given are approximately fitted functions used to characterize the profiles. Effective areas which may be used to relate the total beam energy to

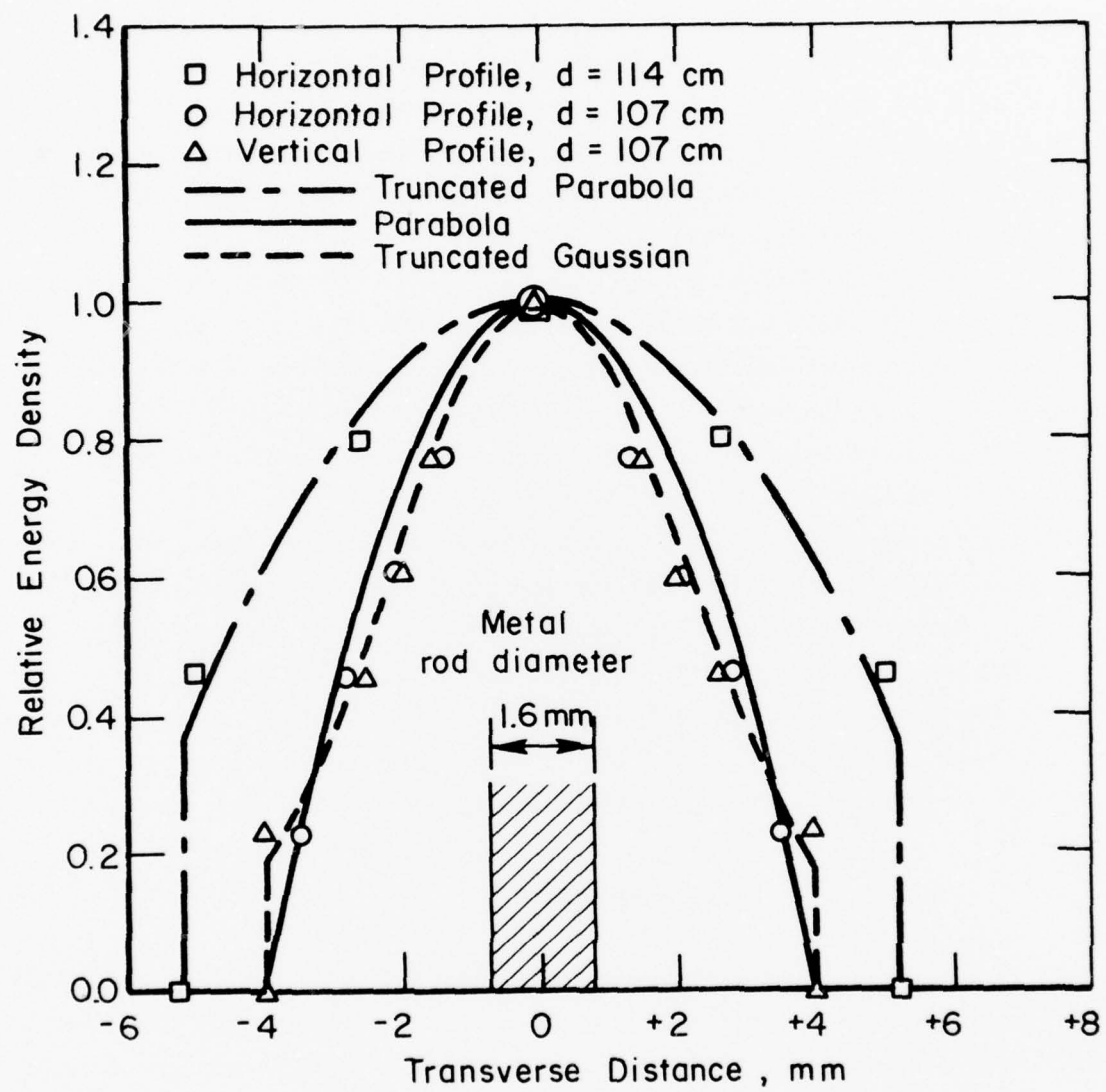


FIGURE 2. MEASURED TARGET PLANE BEAM PROFILES FOR  $\text{CO}_2$  LASER IRRADIATIONS

the peak energy density were found to be  $A_1(d = 114 \text{ cm}) = 0.58 \text{ cm}^2 \pm 10\%$  and  $A_2(d = 107 \text{ cm}) = 0.25 \text{ cm}^2 \pm 10\%$ , where  $d$  is the lens-to-target distance. Also shown in the figure is the diameter of the metal rod sample from which it can be seen that a 5% variation in energy density across the target surface would be expected for an aligned sample ( $d = 107 \text{ cm}$ ) and as much as 40% for a misaligned sample. In the larger spot profile, the alignment sensitivity was much less.

EXPERIMENTAL RESULTS

Using the apparatus and approach discussed in the previous section, irradiations were performed to obtain basic data on the transient reflectivity of metals subjected to intense  $10.6\text{-}\mu\text{m}$  laser pulses. Initial experiments were conducted with the metal in the form of a thin film deposited on a smooth quartz substrate. The smooth, thin film approaches ideal geometry conditions and simulates, to some extent, the thin lamination-type defects important in LSD-wave initiation. The most fruitful experiments were conducted with polished solid rods of several pure metals. Anomalous reflectivity transients were discovered which are highly material dependent. A limited number of aluminum and titanium alloy irradiations were also performed and definite alloy effects were observed. The details of these experiments are discussed in sequence in the following subsections.

Thin-Film Aluminum Irradiations

In this series of experiments, quartz rods of 0.22-cm-diameter were ground flat and polished on one end to serve as substrates for production and irradiation of thin aluminum films. Prior to each irradiation, a fresh polished-quartz rod was cleaned ultrasonically in detergent for 12 minutes, rinsed with distilled water, dried in a dry helium stream, and placed immediately in the vacuum chamber with the flat end facing the tungsten deposition boat. The system was pumped and discharge cleaned at 0.1 Torr argon for 5 minutes. Aluminum films were deposited at pressure levels near  $5 \times 10^{-6}$  Torr with deposition rates in the 40-60-nm/min range. Typical total thicknesses were in the 115-125-nm range. The sample holder was then rotated into the irradiation position by means of mechanical feedthroughs and the irradiation sequence was begun immediately under vacuum conditions.

Typically the irradiation sequence began with 3-7 pulses at low target energy densities ( $< 1 \text{ J/cm}^2$ ) to establish the baseline pulse shape for the particular target alignment. These pulses were followed by a single pulse at an energy density for which the reflectivity transient was desired. Typical aluminum film reflectivity data are presented in Figure 3. To the left of the figure, graphs of the incident and reflected laser pulse shapes drawn from

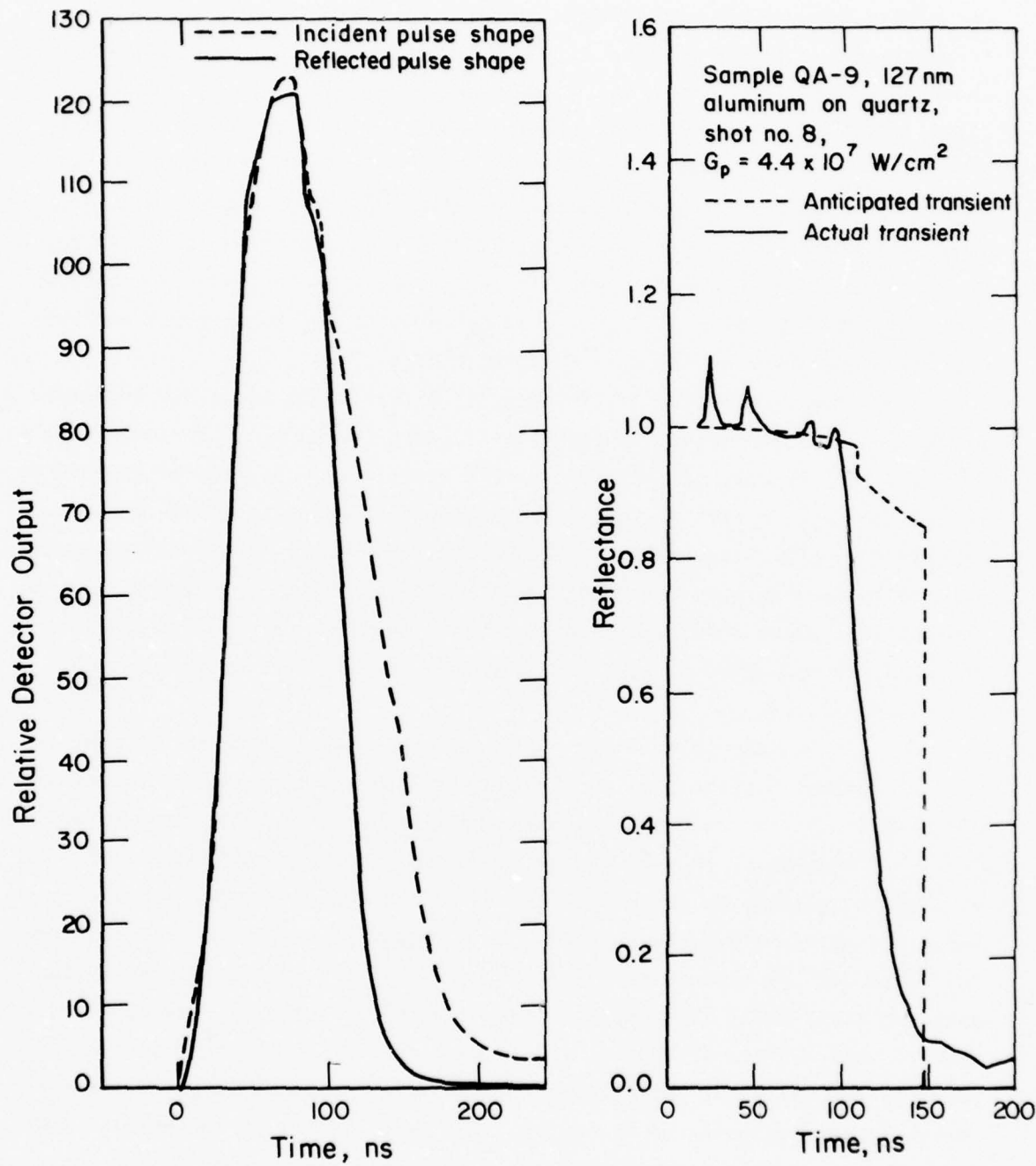


FIGURE 3. REFLECTIVITY RESULTS FOR ALUMINUM FILM WITH PEAK POWER DENSITY ABOVE THRESHOLD FOR COMPLETE FILM REMOVAL

digitized oscilloscope records of sample QA-9 irradiations are presented. The dashed line is the pulse shape recorded for a low-intensity nondamaging irradiation and the solid line is the reflected signal for an incident energy density of  $4.4 \text{ J/cm}^2$  ( $4.4 \times 10^7 \text{ W/cm}^2$  peak power density). The reflected signal has been multiplied by a single constant which was selected to match the rising portion of the reflected signal to that of the incident pulse shape. In most cases, this constant was within 5-10% of the ratio determined from calorimeter readings. To the right of the figure is the computed ratio of the adjusted data which is the inferred time-dependent relative specular reflectivity. The fluctuation from unity near the beginning gives an indication of the 5% pulse-to-pulse reproducibility.

From examination of the specular reflectivity transient of Figure 3, it is clear that no significant structure exists which would be indicative of a finite jump in absorptivity at the melt transition. Rather, it appears as though the film reaches a critical condition and the heating rate becomes anomalously large, i.e. nearly total absorption. The reflectivity transient expected from classical theory is shown qualitatively by the dashed line in the figure. Under such conditions, the film would be expected to vaporize and this was confirmed by the very bright luminosity observed with open-shutter photography.

It was the intent of the study of thin aluminum films to investigate the details of the jump in absorptivity and the temperature dependence of absorptivity in the melt region for varying conditions of incident energy density. Because of the apparently anomalous jump in absorptivity, however, it was not possible to produce a film which had achieved melt, but not been vaporized or blown off the surface. In 12 separate sample irradiations conducted at various beam intensities, the reflectivity data consistently indicated an anomalously large drop in specular reflectivity for energy density above a well-defined threshold. These data are summarized in Figure 4 which presents the timing of the falling portion of the reflectivity transient relative to the beginning of the pulse. The dark filling of the circles indicates the approximate fraction of the aluminum film remaining on the quartz surface. Because the thicknesses of the films vary somewhat from sample to sample, all values of incident energy density have been adjusted slightly to those values which would correspond to equivalent heating in a 120-nm-thick film. A threshold for the anomalous reflectivity effect is noted which

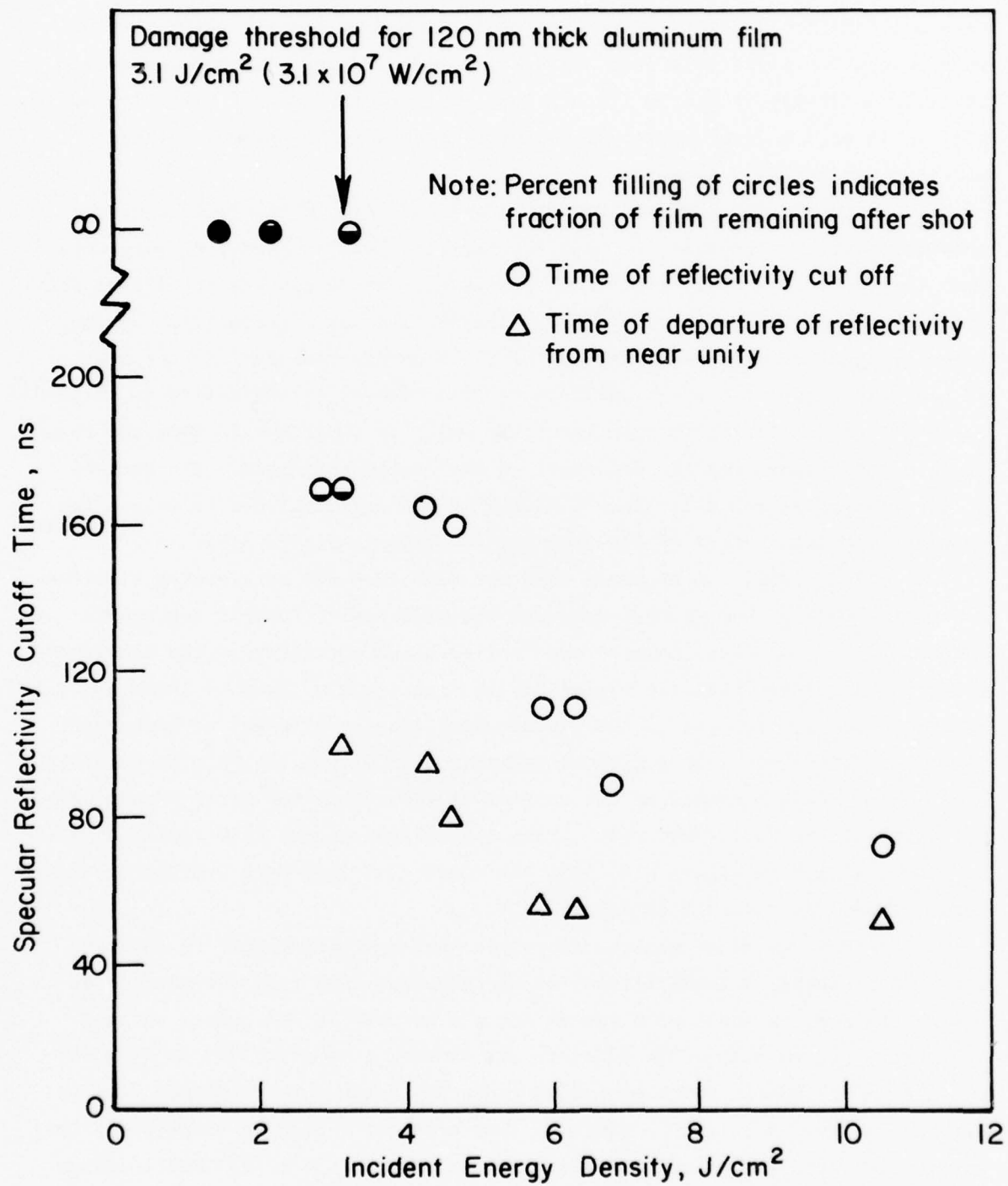


FIGURE 4. TIMING OF REFLECTIVITY CUTOFF FOR ALUMINUM FILM IRRADIATIONS (DATA ADJUSTED FOR EQUIVALENT ENERGY DENSITY AT 120 nm THICKNESS)

corresponds well to the observed film damage threshold,  $3.1 \text{ J/cm}^2$ . The film melt threshold for a 100-nm film calculated from heat-transfer theory (accounting for conduction into the quartz) is  $2.3 \text{ J/cm}^2$ . If the correction for film thickness is nearly linear, the predicted threshold for the 120-nm film would be  $2.8 \text{ J/cm}^2$ , which agrees with the observed damage threshold within experimental accuracy.

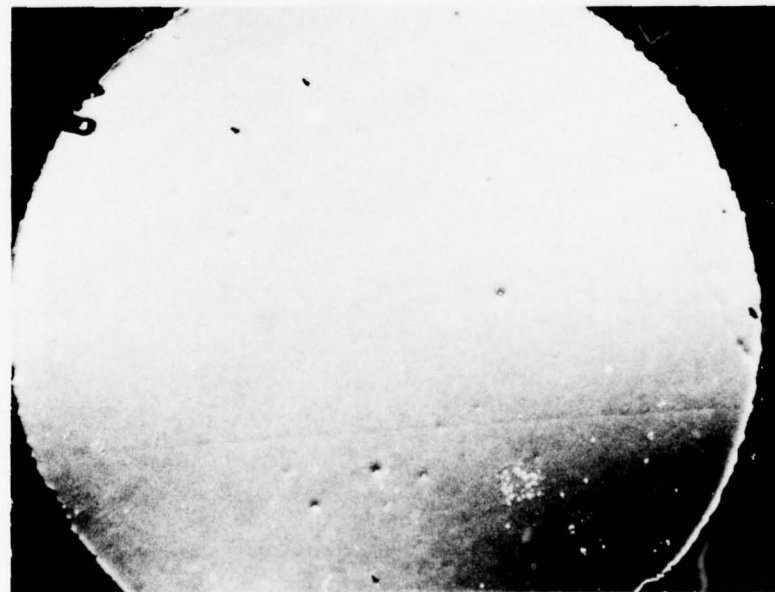
Two of the thin film samples (QA-5 and QA-8) were examined microscopically after irradiation. QA-5 was irradiated at an energy density very near threshold,  $2.3 \text{ J/cm}^2$  ( $3.2 \text{ J/cm}^2$  equivalent energy density for 120-nm film) and QA-8 was irradiated at  $1.8 \text{ J/cm}^2$ . Sample QA-5 was affected more by the laser irradiation with more than 50% of the aluminum removed from the quartz as shown in Figure 5(a). The pattern of film removal is indicative of the small scale (5-10%) variation in beam intensity which is superimposed upon the beam profile and illustrates the sharpness of the damage threshold. The surface of QA-8 showed very little overall effect of the irradiation with only a few possible localized areas of disturbance, as noted in Figure 5(b).

The surface of Specimen QA-5 was also examined by scanning electron microscopy (SEM). The general features included small circular regions in which the film had been ruptured and "rolled back" outward from the center of the circle. These areas are marked "A" in Figure 6(a). Many of these holes had a small speck of material in the center which appears globular at high magnification. These might be a glob of melted aluminum from the film or possibly an  $\text{Al}_2\text{O}_3$  particle retained on the surface of the quartz rod after mechanical polishing of the end of the rod. Other disruptions in the film appear as slits or tears as seen in Figure 6(b) with the edges just laid back instead of rolled back. These are marked B in Figure 6(b).

These circular regions of rolled back material appear to initiate first as blisters, a local lifting of the aluminum film from the surface of the quartz rod. A trail of blisters along a scratch in the quartz surface is seen in Figure 6(a). The blisters are evidently able to lift quite a distance from the quartz surface without rupturing because the aluminum film is hot and has good ductility. However, they eventually reach a point where they rupture near the top of the blister as shown at A in Figure 7. The location of the rupture at the top of the blister may be partly because the temperature of the film must increase rapidly if it lifts away from the surface during the pulse. The temperature would be highest at the top of the blister, farthest

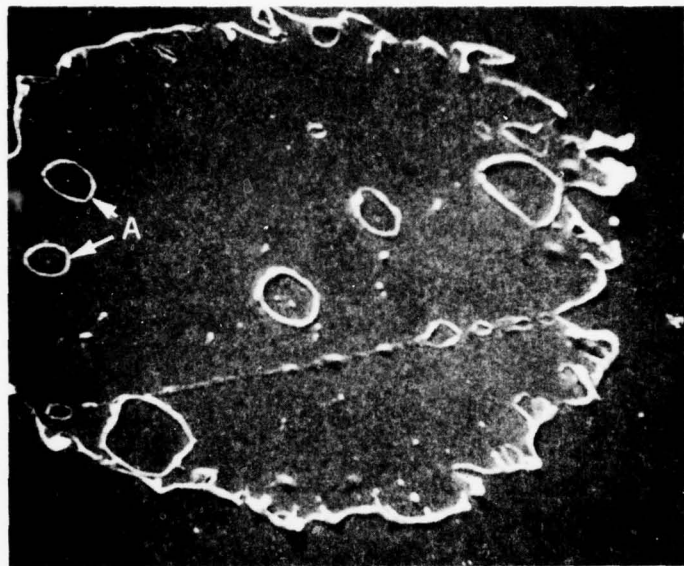


50X  
(a) Sample QA5--Peak Power Density,  $2.3 \times 10^7$  W/cm<sup>2</sup>,  
Film Thickness 87 nm



50X  
(b) Sample QA8--Peak Power Density,  $1.8 \times 10^7$  W/cm<sup>2</sup>,  
Film Thickness, 126 nm

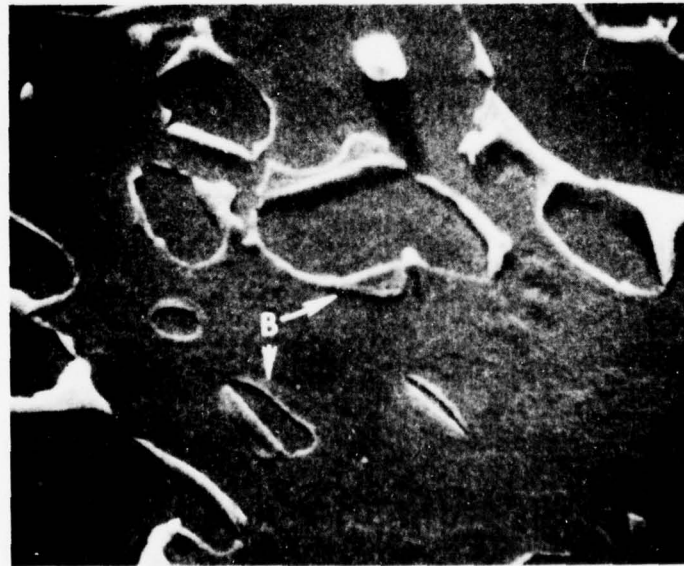
FIGURE 5. LOW MAGNIFICATION VIEWS OF THE LASER-IRRADIATED SURFACES OF  
ALUMINUM FILMS DEPOSITED ON POLISHED FUSED QUARTZ  
(NOMARSKI LIGHTING)



#19392

500X

(a) General Appearance of Aluminum Film Showing Clear Areas with Rolled Back Edges. A Indicates Clear Areas with Particle in Center.



#19394

2000X

(b) Area in Aluminum Film Having Edges of Clear Areas Laid Back. B Indicates These Areas.

FIGURE 6. APPEARANCE OF SMALL RUPTURED AREAS IN THE ALUMINUM FILM AFTER LASER IRRADIATION, SAMPLE QA-5

from the "cooled" perimeter. After the top of the blister tears, it appears that the edges of the film then usually roll back, exposing the quartz surface. These rolled-up edges, having lost thermal contact with the substrate, become hot enough to melt as clearly shown at B in Figure 7. The rolling up must occur rapidly since in some areas where melting was observed the droplets are thrown forward some distance in the direction the film is being thrown back, Figure 8.

The detailed reasons for and timing of the lifting of the aluminum film from the quartz substrate is not understood. The lifting appears to be caused by gas pressure under the film. This could be caused by heat conducted into the substrate or deposited directly during a transient dielectric transition of the film. Attempts to determine by metallographic methods whether or not the film remaining intact had undergone melting were unsuccessful because of the small film thicknesses. Because of these uncertainties, the remaining experiments in the program were conducted with bulk metal samples.

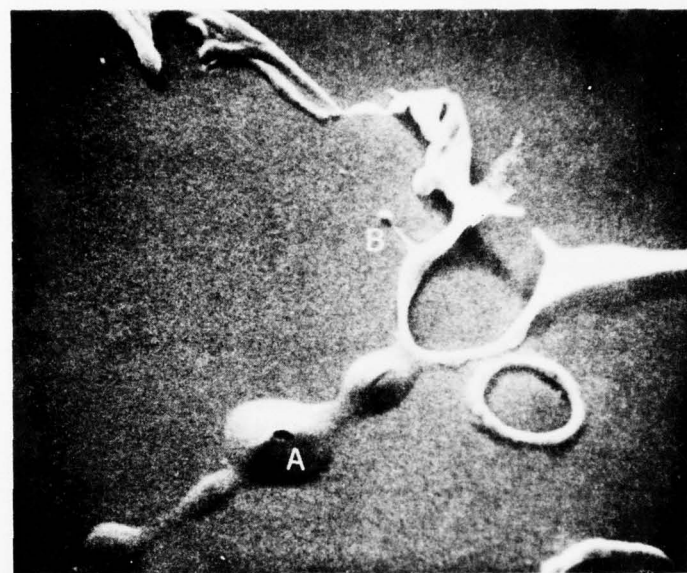
#### Bulk Aluminum Irradiations

To further explore the transient reflectivity behavior of pure aluminum subjected to intense  $10.6\text{-}\mu\text{m}$  laser pulses, bulk aluminum samples were subjected to substantially the same irradiation procedures as those used for the thin-film experiments.\* The samples were cut from 1.6-mm-diameter wire of deposition-grade polycrystalline aluminum (0.99999 pure). One end of each sample was ground flat and mechanically polished by standard metallographic techniques. Ultrasonic cleaning was not used for the bulk samples as this was found to damage the surface. A detergent wash followed by a distilled water rinse and drying in a helium stream was the only clearing procedure employed. Following cleaning, the sample was mounted in the reflectivity apparatus and optically aligned. The chamber was pumped to pressures in the  $1\text{-}5 \times 10^{-6}$  Torr range for all irradiations.

#### Reflectivity Results

A series of eight aluminum samples were irradiated using various levels of beam intensity and sequences of pulses. Initial results<sup>(16)</sup> revealed an

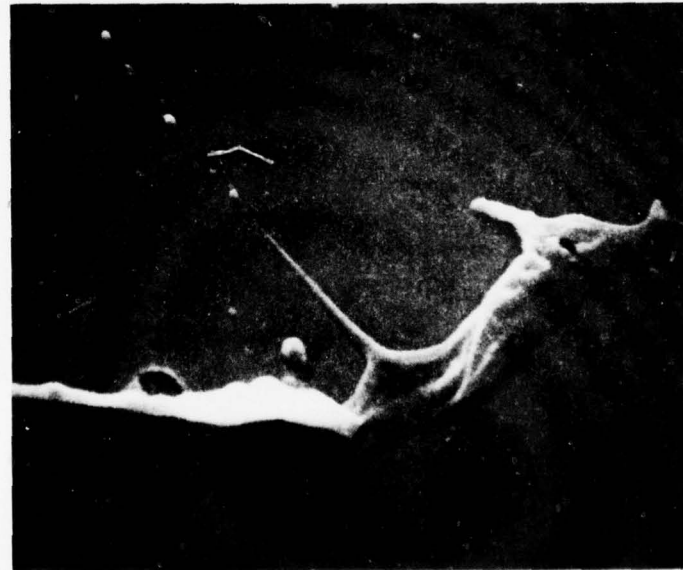
\* A minor difference was the effective pulse length which was in the 50-70 ns range for the bulk sample irradiations.



#19391

2000X

FIGURE 7. REGION OF LASER-IRRADIATED ALUMINUM FILM SHOWING THE FORMATION OF BLISTERS, RUP-TURING OF A BLISTER AT A, AND MELTING AT B. SAMPLE QA-5.



#19354

2000X

FIGURE 8. MELTING OF THE ROLLED-UP EDGE OF THE ALUMINUM FILM AND THROWING OF THE DROPLETS IN THE DIRECTION OF ROLLING. SAMPLE QA-5.

anomalous drop in specular reflectivity during the pulse followed by nearly complete recovery of reflectivity at the end of the pulse. This effect is illustrated in Figure 9 which presents reflectivity results for Sample A-4. To the left of the figure the digitized oscilloscope records are presented for the first pulse on the sample which was well above the threshold for reflectivity change. Prior to this irradiation, the surface was "conditioned" by several irradiation at intensities below the melt threshold and two irradiations at intensities very near this threshold. The threshold for achieving melt on the surface has been calculated numerically to be near  $3.0 \times 10^8$  W/cm<sup>2</sup> as discussed in a subsequent section. As can be seen in the figure, the reflected signal drops sharply to zero near the peak of the incident radiation and remains low until late in the pulse, whereupon the reflected signal regains nearly the shape of the incident pulse. The complete cutoff of reflected radiation is a reproducible effect for irradiations in which a conditioned surface is first exposed to peak power densities well exceeding the melt threshold. Very faint luminosity on the sample surface was correlated with the reflectivity cutoff phenomenon. Second and succeeding irradiations at the same power density produced no luminosity and no complete cutoff of reflectivity, although an anomalously large reduction in reflectivity was observed. It should be noted that the loss in specular reflectivity here is not likely a result of diffuse scattering, because the sample exhibits only very subtle surface damage and no significant decrease in low-intensity specular reflectivity from shot to shot. The ratio of the reflected signal to incident signal for this irradiation (Shot No. 9) and a subsequent irradiation (Shot No. 10) were calculated from the digitized data and are presented on the right side of Figure 9. As can be seen in the figure, the reflectivity for Shot No. 10 drops as low as 35% during the pulse, but recovers to nearly full reflectivity late in the pulse. The effect is reproducible once an initial "stabilizing" shot has been made which greatly exceeds the melt threshold. It is believed that Shot No. 10 is representative of the true reflectivity behavior of the bulk aluminum surface for temperatures above the melt point. The cut-off effect on the first shot is not well understood, but may be triggered by absorption at impurities (imbedded in the surface during polishing).

Also presented in Figure 9 is the reflectivity transient for the first pulse on the sample which produced a deviation from unity reflectance (Shot No. 7, peak power density,  $3.1 \times 10^8$  W/cm<sup>2</sup>). As noted in the figure,

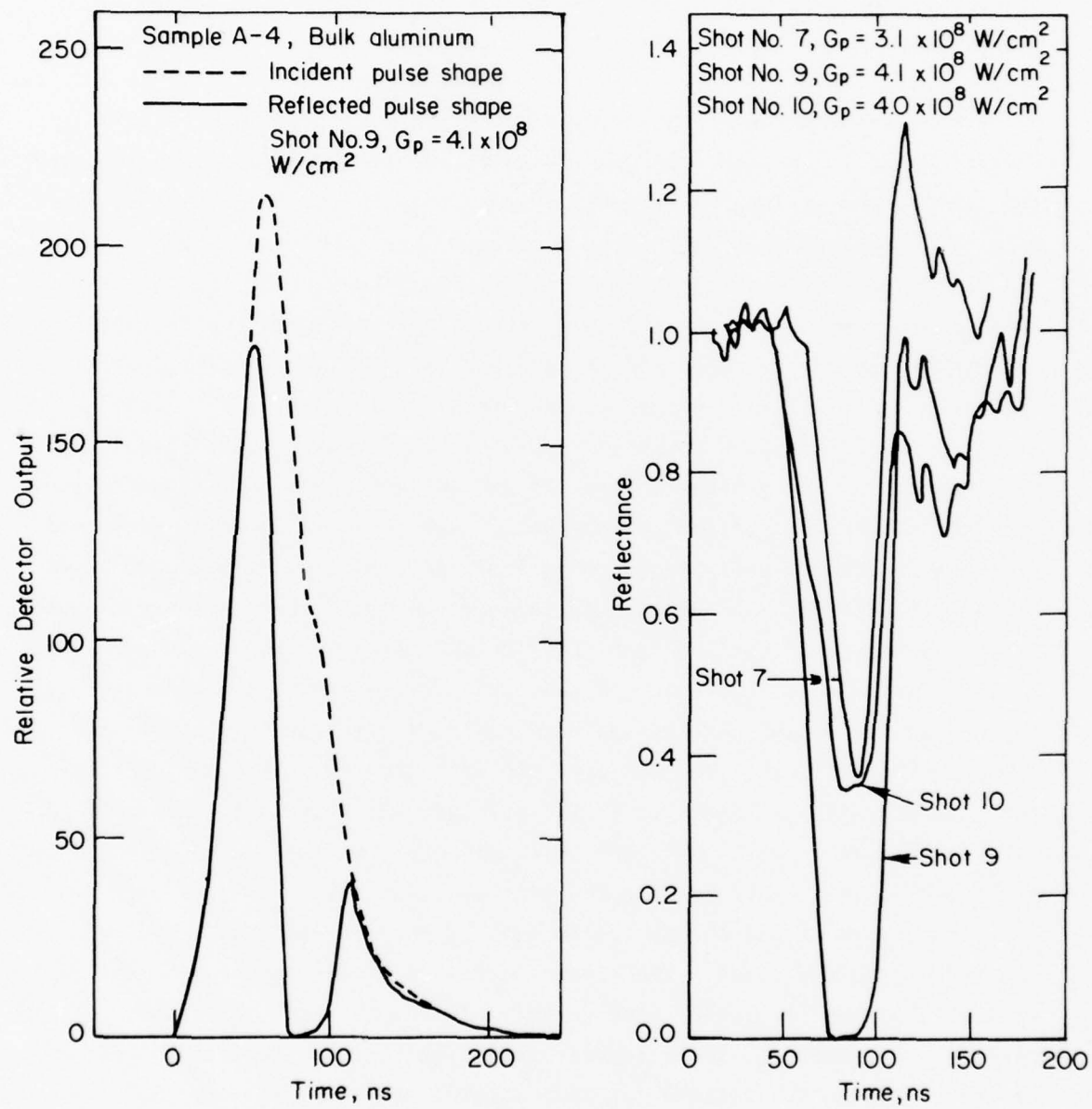


FIGURE 9. SPECULAR REFLECTIVITY TRANSIENTS FOR BULK ALUMINUM SAMPLE A-4

the reflectivity drops at a later time in the pulse (corresponding to the lower intensity) but achieves a low value near 0.35. The "over-recovery" late in the pulse may be a noise effect. It should be noted that this transient was not reproduced on the subsequent pulse at the same intensity, but a "curing" effect was noted wherein the reflectivity did not deviate nearly as much from unity.

From these results, it was clear that both a distinctive reflectivity cutoff effect and an anomalous reflectivity transient were being observed, but the effect of repeated pulsing required additional study. Several additional samples were irradiated in an attempt to understand these effects. Table 1 summarizes the conditioning sequences and reflectivity results for the aluminum samples. Samples A-8 and A-9 were removed from vacuum for examination and were subsequently reirradiated, hence the designations A-8(a) and A-8(b). Consideration of these results leads to the following conclusions.

- The threshold for the cutoff phenomenon is strongly dependent upon the conditioning sequence, but almost always was above the melt threshold (note A-7 exception)
- The cutoff effect is always "cured" by a second pulse at the same peak power density
- Cutoff can be observed more than once on the same sample if the beam intensity is raised
- Cutoff is essentially a base material effect as opposed to gas desorption or oxide absorption as noted from the fact that Sample A-8 did not exhibit cutoff after exposure to air between the A-8(a) and A-8(b) series irradiations
- The anomalous reflectivity transient is reproducible for a given set of conditions once the surface is "stabilized" by a pulse producing the cutoff effect
- Accumulation of a number of pulses at high intensity will degrade the transient reflectivity.

The latter effect is illustrated in Figure 10 which shows reflectivity data for Sample A-8(b) near the end of a sequence of pulses at high intensity. The minimum reflectivity is in the 0.05 to 0.20 range and recovery is incomplete during the pulse. Nearly complete recovery must occur after the pulse as there is little degradation in low-intensity reflectance.

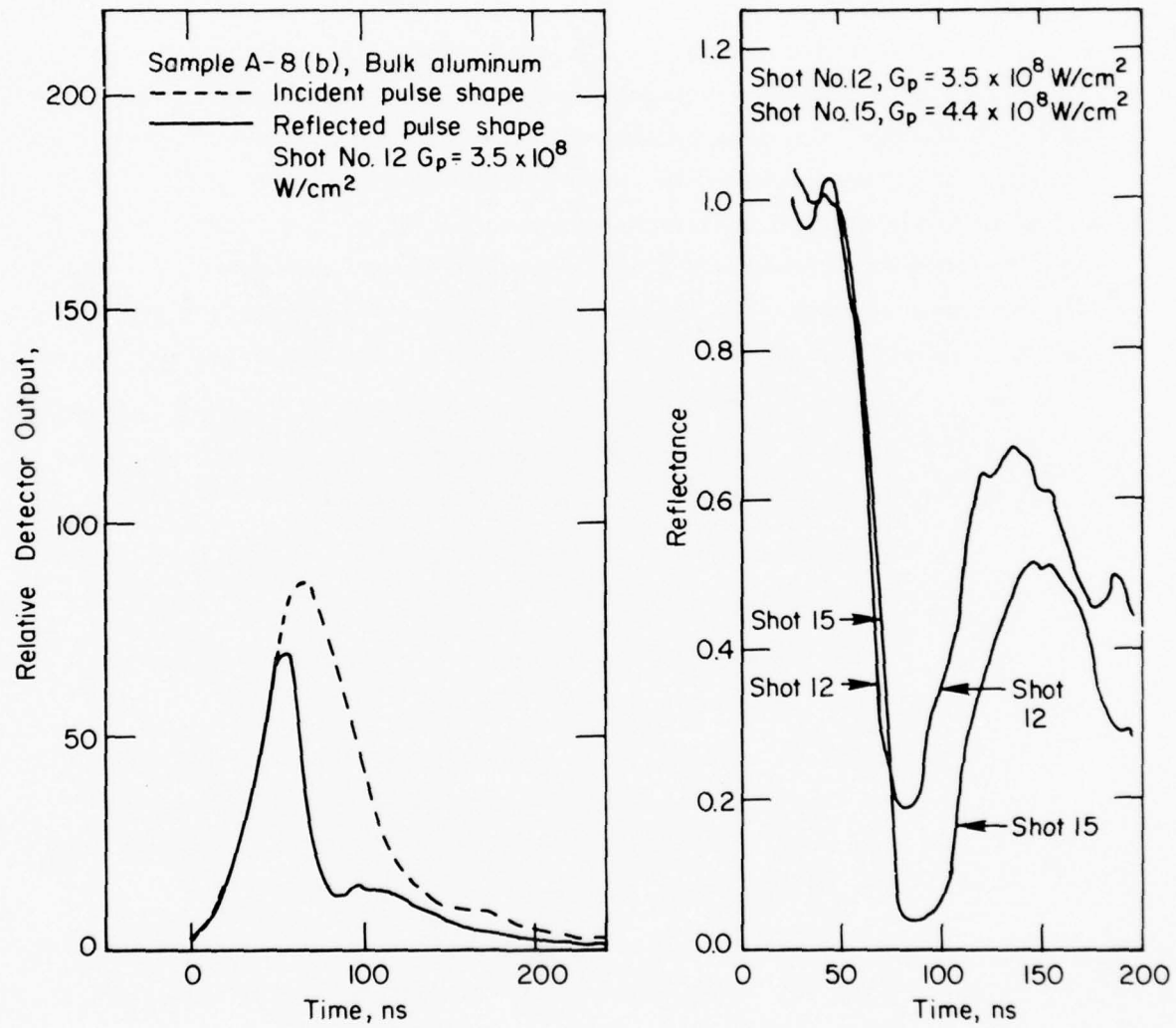


FIGURE 10. SPECULAR REFLECTIVITY TRANSIENTS FOR BULK ALUMINUM SAMPLE A-8(b)

TABLE 1. SUMMARY OF BULK ALUMINUM IRRADIATIONS

Sample	Conditioning Sequence		Anomalous Reflectivity Effect (a)	Number of Pulses above $3.0 \times 10^8 \text{ W/cm}^2$	Final Damage (a)
	Number of Shots	$C_p, \text{W/cm}^2$			
A-1	26	$\leq 1.6 \times 10^8$	None	0	None
A-2	4	$6.3-6.8 \times 10^7$	None	0	Strong grain relief
	26	$2.1-2.5 \times 10^8$			
A-3	4	$7.4 \times 10^7$	Cutoff observed at $3.7 \times 10^8 \text{ W/cm}^2$ , no additional pulses	1	Bullseye craters, slip bands, no scratches, grain relief, undulation, grain differentiation, microwrinkles
	3	$1.8 \times 10^8$			
	1	$2.2 \times 10^8$			
	1	$2.8 \times 10^8$			
A-4	2	$1.1 \times 10^8$	Strong effect followed by curing at $3.1 \times 10^8 \text{ W/cm}^2$ (2 pulses) cut- off followed by strong effect once at $4.0 \times 10^8 \text{ W/cm}^2$ (2 pulses)	4	Same as A-3
	2	$1.6 \times 10^8$			
	1	$1.9 \times 10^8$			
	1	$2.6 \times 10^8$			
A-5	None		Cutoff observed at $3.1 \times 10^8 \text{ W/cm}^2$ (1 pulse)	1	Same as A-3
A-6	None		Little or no effect at $1.3 \times 10^8 \text{ W/cm}^2$ (1 pulse)	0	Slight grain relief

TABLE 1. (Continued)

Sample	Conditioning Sequence		Anomalous Reflectivity Effect (a)	Number of Pulses above $3.0 \times 10^8 \text{ W/cm}^2$	Final Damage (a)
	Number of Shots	$G_p, \text{W/cm}^2$			
A-7	3	$6.8 \times 10^7$	Cutoff observed (with slow fall time) at $2.0 \times 10^8 \text{ W/cm}^2$ (1 pulse)	0	Grain relief
A-8 (a)	3	$1.1 \times 10^8$	Cutoff observed followed by curing on second shot at $3.4 \times 10^8 \text{ W/cm}^2$ (2 pulses), cutoff observed followed by weak effect twice at $4.2 \times 10^8 \text{ W/cm}^2$ (3 pulses)	5	Same as A-3, but greater surface undulation, loss of grain texture differences
A-8 (b)	3	$9.1 \times 10^7$	Weak effect observed at $2.7 \times 10^8 \text{ W/cm}^2$ (1 pulse), strong effect twice at $3.5 \times 10^8 \text{ W/cm}^2$ (2 pulses) strong effect five times at $4.2 \times 10^8 \text{ W/cm}^2$ (5 pulses) minimum reflectivity decreasing and recovery incomplete during pulse	7 (12 pulses cumulative)	Same as A-8(a), many bullseye craters obliterated
A-9 (a)	13	$<3 \times 10^8$	None	0	Grain relief
A-9 (b)	3	$1.1 \times 10^8$	Cutoff observed followed by strong effect 3 times at $3.6 \times 10^8 \text{ W/cm}^2$ (4 pulses), strong effect at $4.2 \times 10^8 \text{ W/cm}^2$ (1 pulse)	5	Same as A-3, some local areas exhibit extremely smooth appearance, except for grain boundaries

Metallographic Examination

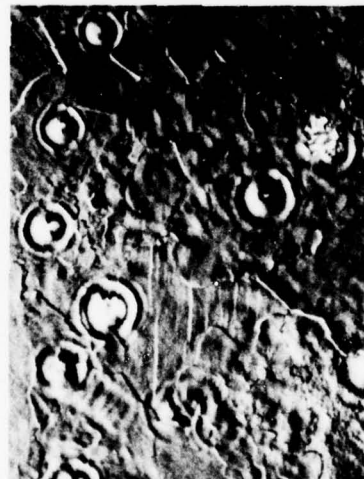
Some of the aluminum samples used in the experiments were examined microscopically to assess changes in surface conditions arising from the irradiations. The surface condition of a typical sample (A-5) before irradiation is shown in the Nomarski micrograph of Fig. 11(a). There is some surface relief of the grains and some residual scratches from polishing. Irradiation of the sample at peak power density above the threshold for the anomalous reflectivity transient produced features indicative of melt on the surface as shown in Fig. 11(b). This figure presents a Nomarski micrograph of the same surface area after a single irradiation at  $3.1 \times 10^8 \text{ W/cm}^2$  peak power density. One feature indicative of melt is the circular structure which appears at several points on the surface. These structures sometimes contain one or more particles in the center, sometimes have a smooth center, or less often, they have a small pit in the center. The center of the structure or "bullseye" crater is often on a grain boundary. Similar features have been observed recently by Decker et al.<sup>(17)</sup> on copper samples subjected to  $10.6 \mu\text{m}$  radiation. These features are apparently centers of absorption due to imbedded debris or perhaps subsurface porosity. It is conjectured that the surrounding ring structure of a bullseye crater is caused by a radially-propagating surface-shear wave which is preserved by the rapid quenching of the surface melt layer. The characteristic wavelength of the oscillations was typically  $2-4 \mu\text{m}$  which indicates that the structure did not arise from optical interference effects.<sup>(2)</sup> From multiple irradiation experiments, it was found that these features are slowly obliterated after the first pulse.

Other features seen in Fig. 11(b) include enhanced surface relief of grain boundaries, slip banding, random undulation of the surface, and a tendency for differentiation in the surface texture of individual grains. The enhanced surface relief of grains was observed also for samples irradiated at peak power densities well into the melt regime. This fact and the clear indication that grain boundary relief lines are observed to cut across the bullseye craters suggest that epitaxial regrowth followed by thermal etching of the grain boundary or even possibly grain boundary sliding under the influence of thermal stress occurs upon cooling of the surface. Additional evidence of stress is seen in slip lines which also cut across the bullseye craters when present. Slip-banding in laser-irradiated aluminum single crystals has been observed



500X

(a) Before Irradiation



500X

(b) After Irradiation

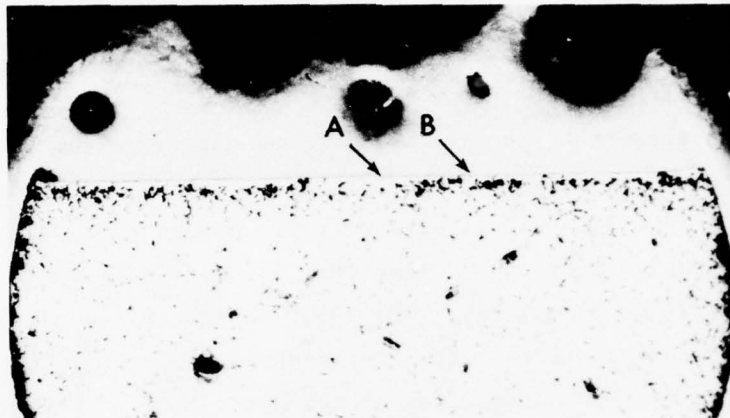
FIGURE 11. APPEARANCE OF ALUMINUM SAMPLE A-5 BEFORE AND AFTER IRRADIATION  
AT  $3.1 \times 10^8$  W/cm<sup>2</sup> PEAK POWER DENSITY (1 PULSE)

previously by Porteus et al.;<sup>(18)</sup> however, in their case, evaporative compressive stresses were cited as the cause of slip. The random undulation of the surface and absence of polishing scratches suggest that homogeneous melting has occurred. The characteristic wavelength for undulation increases for increased peak power density above the melt threshold, indicating thicker melt layers.

In an attempt to confirm melting and determine the heat-affected zone, samples which had been exposed to many pulses above the theoretical melt threshold were examined in more detail. Sample A-8, which was irradiated above the melt threshold 12 times, was mounted, taper sectioned, and examined by light microscopy. The taper section gives a 10:1 increase in apparent depth of features below the irradiated surface. Evidence of surface melting was sought, but because of the difficulty of etching pure aluminum to bring out the grain microstructure, the results were not definitive. It was not possible to identify melted regions based on grain structure differences. There were other interesting observations, however. Figure 12(a) shows a low magnification view of the tapered specimen section encased in a nickel plate. The irradiated surface is intersected by the taper plane, at the straight edge. In the figure, it is noted that there is an uneven distribution of voids (dark points) below the laser irradiated surface. Most of these were observed to be voids or pores when examined in the as-polished condition, although some of them appear to be etch pits. The dark points around the curved periphery of the section (unirradiated surface) are etch pits and were not visible as voids in the as-polished condition. The higher magnification view given in Figure 12(b) shows these voids and the void-free region just under the surface more clearly. The thickness of the void-free region is approximately  $1 \mu\text{m}$  which is consistent with the anticipated melt depth for these short pulses ( $1\text{-}4 \mu\text{m}$ ).

The taper section also showed in profile features previously observed by surface examination. What appears in the cross section as one or possibly two overlapping craters is shown in Figure 13(a). The low points are indicated at A. Another crater, or pit, in the irradiated surface appears in profile at B in Figure 13(b). These areas are also indicated by A and B in Figure 12(a).

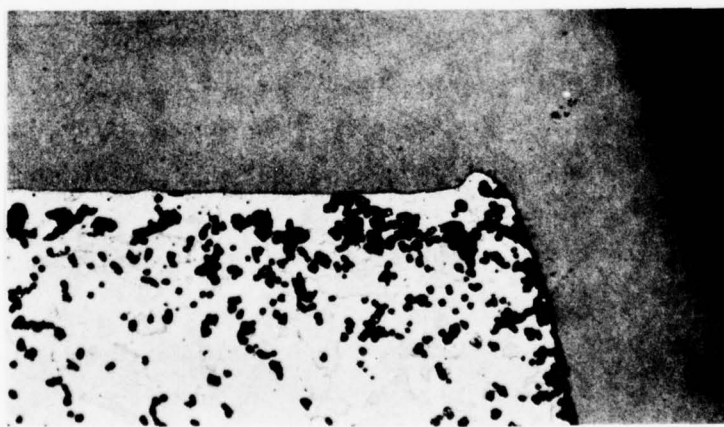
Sample A-9 was also examined microscopically. Figure 14(a) presents a low-magnification view of the irradiated surface. A high-magnification view of a 10:1 taper section through the same surface (unetched) is shown in



4J769

75X

(a) General View Showing a Pore-Free Zone Just Under the  
Irradiated Surface and the Heavy Concentration of Pores  
Below It.

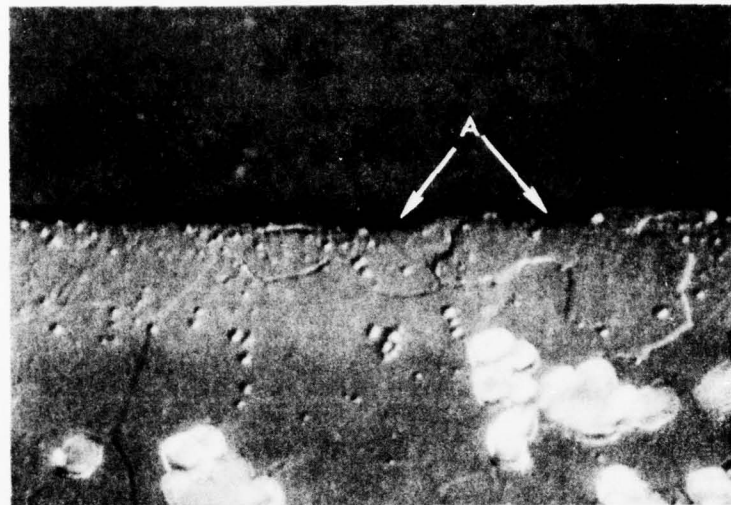


4J770

250X

(b) View of Pore-Free Zone Near the Irradiated Surface

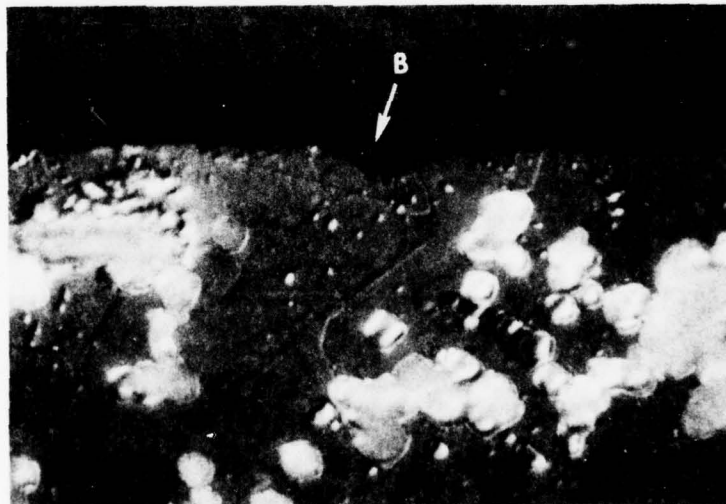
FIGURE 12. TAPER SECTION THROUGH A LASER-IRRADIATED ALUMINUM SURFACE  
(SAMPLE A-8). THE SECTION INTERSECTS THE IRRADIATED SURFACE  
ALONG THE FLAT EDGE. THE SAMPLE WAS PLATED WITH NICKEL BEFORE  
METALLOGRAPHY.



4J771

1500X

(a) Irregularity Profiles in Irradiated Surface Which May be Craters Marked by A.



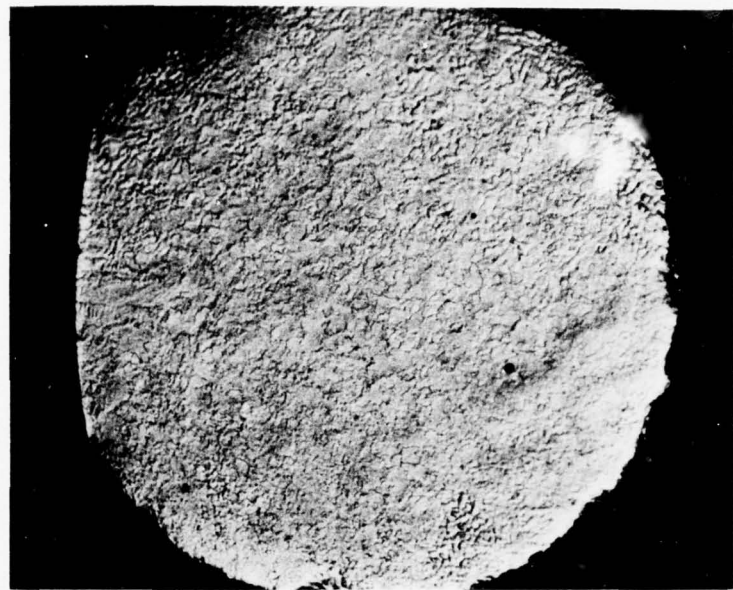
4J772

1500X

(b) Profile of What Appears to be a Pore in the Irradiated Surface at B.

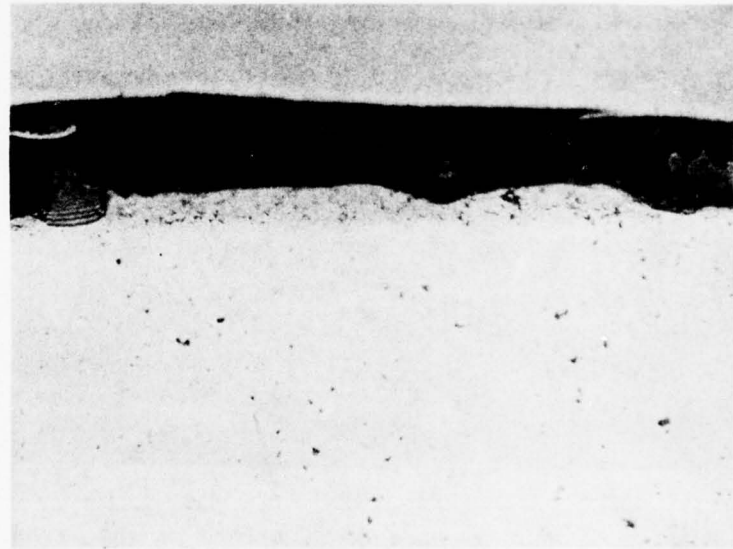
FIGURE 13. PROFILES OF THE IRRADIATED SURFACE SHOWING GRAIN BOUNDARIES AND POROSITY (SAMPLE A-8).

The regions marked A and B are also indicated in Figure 12(a). Micrographs taken with Nomarski differential interference contrast.



60X

(a) Irradiated Surface (Nomarski Lighting)



800X

(b) As-Polished View of 10:1 Taper Section Through  
Irradiated Surface. Melt Layer is Seen Below  
Dark Band.

FIGURE 14. VIEWS OF SAMPLE A-9 AFTER IRRADIATION

Figure 14(b). Evidence of a melt layer is seen below the dark band (mounting material). This layer does not extend over the entire surface of the sample, but appears in several patches. The maximum thickness of the layer is 0.8  $\mu$ m.

#### Irradiations of Other Metals and Alloys

To confirm the universality of the anomalous reflectivity transients observed for aluminum, irradiations of other pure metals and two alloys in bulk form were conducted. The pure metals were cut from 1.6-mm-diameter deposition-grade polycrystalline wire and were prepared, for the most part, in the same manner as were the aluminum samples. It was found necessary to electro-polish the copper sample after mechanical polishing in order to eliminate scratches. The alloy samples were trepanned from sheet stock, polished, and mounted on support rods. These samples were 2.4-mm in diameter and did not receive as uniform irradiance as did the other samples. All samples were conditioned with low-intensity irradiations in sequences similar to those indicated in Table 1.

All samples exhibited a transient change in reflectivity, but the nature of the transient and threshold levels were highly material dependent. Results for the various samples are summarized below.

#### Pure Copper Results

The reflectivity transients for copper were similar to those of aluminum in that they exhibited a complete cutoff of reflectivity on the first shot at a given level (above a fixed threshold) which was "cured" on the subsequent shot at that level. The curing effect in copper, however, was complete in the sense that no deviation from unity was observed in the reflectivity signal on the second shot at each level. The cutoff effect followed by curing was observed in copper at three successive intensities 3.4, 4.2, and  $5.4 \times 10^8$  W/cm<sup>2</sup>, the latter being the upper limit of the optical arrangement. Local damage was observed on the surface in several isolated regions. The damage features consisted of surface undulation, slip-banding, bullseye craters, and loss of residual scratch marks.

These results are consistent with the picture that the cutoff effect is triggered by impurities (which are hard to avoid in soft materials) or voids which are centers of absorption and are self-healing. The fact that uniform

melting and a stable reflectivity departure from unity were not achieved is consistent with the anticipated high intrinsic damage threshold for copper. The fact that local absorption can trigger complete cutoff of reflectivity is not understood.

#### Pure Iron Results

Reflectivity transients for an iron sample (F-1) are presented in Figure 15. These transients are from three successive pulses at nearly the same intensity. Shot No. 11 is the first pulse on the sample to exhibit the anomalous reflectivity effect and it is noted that complete cutoff does not occur in this case. There is an unusual dip in reflectivity near the minimum similar to that observed at  $1.06 \mu\text{m}$ ,<sup>(5,8)</sup> however, no plateau is observed. The second and third pulses (Shot Nos. 12 and 13) at almost the same intensity are nearly identical to each other and exhibit a slightly higher minimum reflectivity than seen in Shot No. 11. No strong curing effect occurred as did for aluminum. No luminosity was observed on the target surface during any of the irradiations and it is clear that vapor plasma absorption did not cause the anomalous drop in reflectivity.

Following the three pulses discussed above, the sample was removed and examined microscopically. A low magnification view of the surface is shown in Figure 16(a). The dark spots are bullseye craters. The fringe damage pattern near the upper edge has a fringe spacing of about  $10 \mu\text{m}$  and probably results from interference of a surface wave scattered from the edge with the incoming beam.<sup>(2)</sup> Figure 16(b) presents a high magnification view of the same surface and evidence of melt is seen in the undulation of the surface. As in the case of one of the aluminum samples, this apparent melting was not confirmed definitively by examination of the sample in cross section. A taper section through the irradiated surface at nominally a 10:1 taper is shown in Figure 17. The as-polished condition shows that near the surface many of the grain boundaries are defined by fine precipitates or voids (Figure 17(a)) compared to the interior where only inclusions and precipitate particles are visible. In the etched condition, this preferential delineation of the grain boundaries is not as visible (Figure 17(b)). In both Figures 17(a) and 17(b), some of the craters visible on the irradiated surface are visible in profile as shown by the arrows. However, there is no discernable subsurface effect in the vicinity of these craters to indicate melting occurred. It is not clear whether

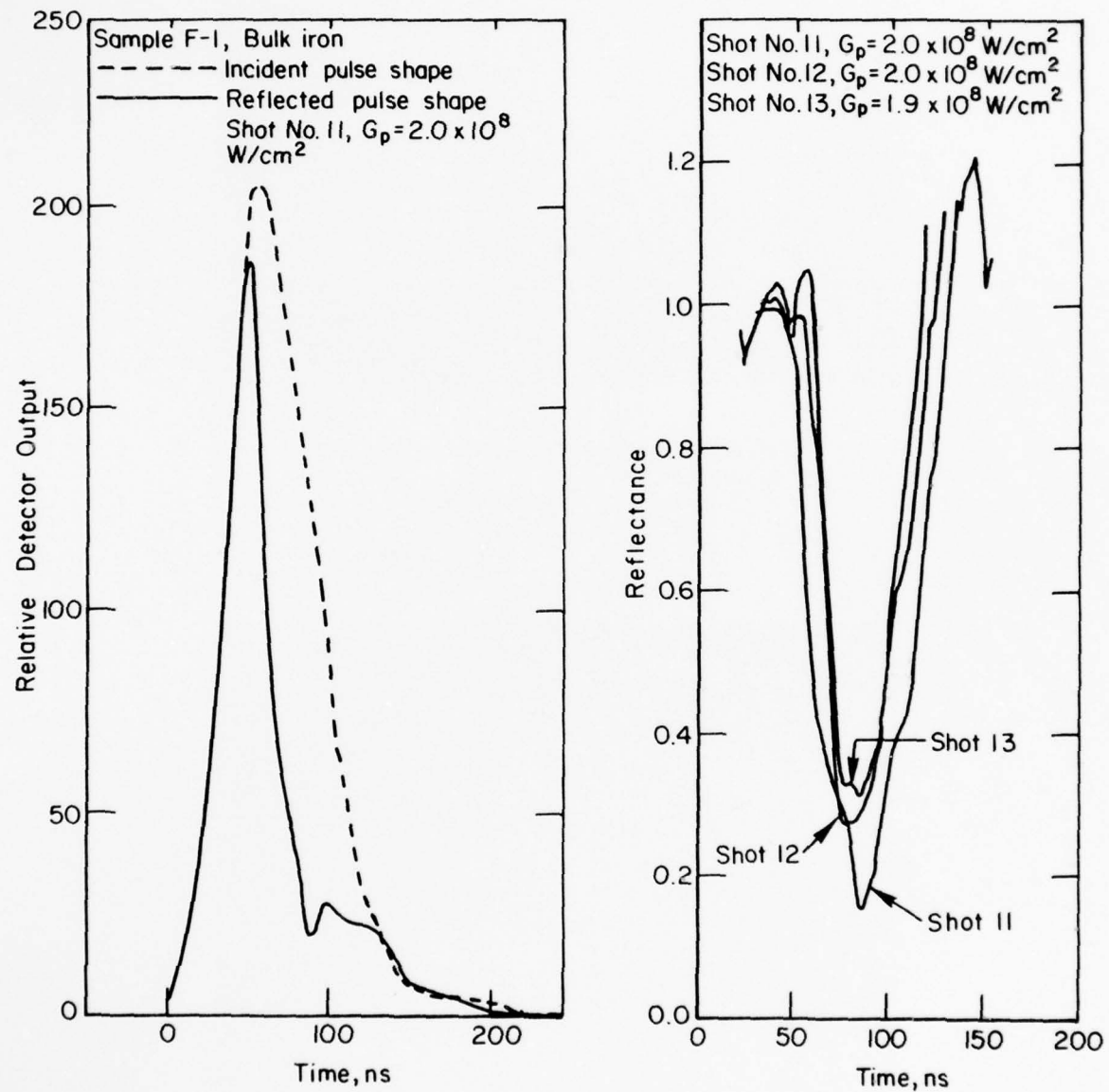
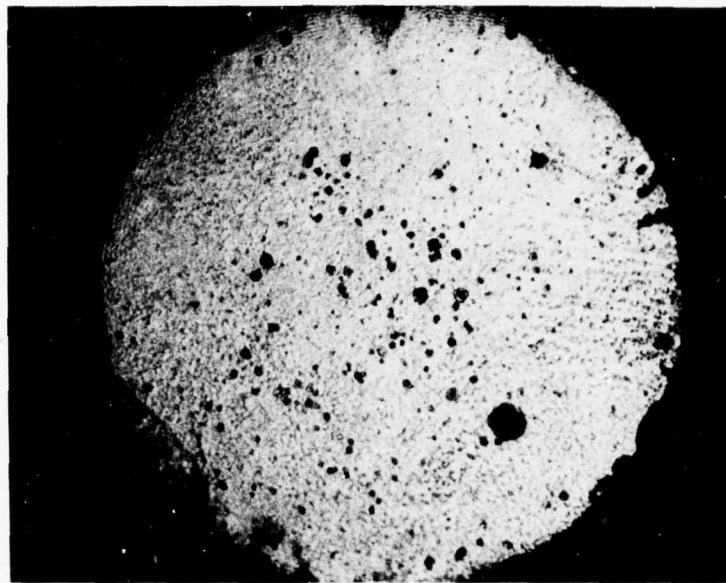
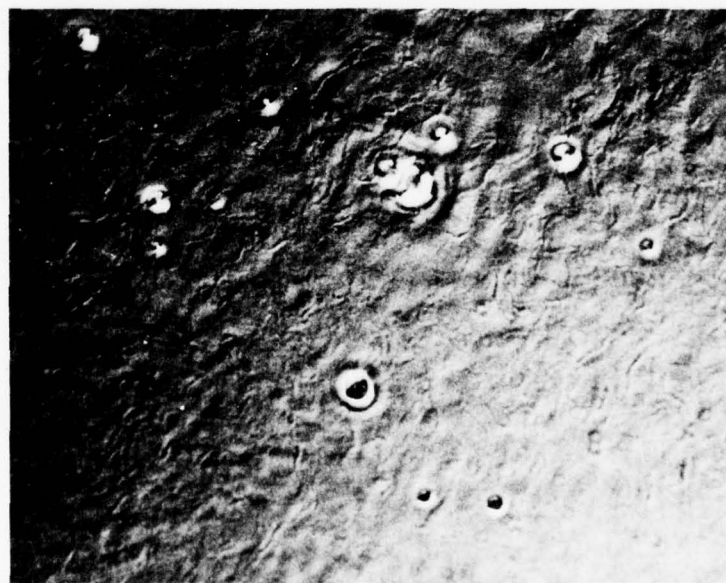


FIGURE 15. SPECULAR REFLECTIVITY TRANSIENTS FOR BULK IRON SAMPLE F-1



60X

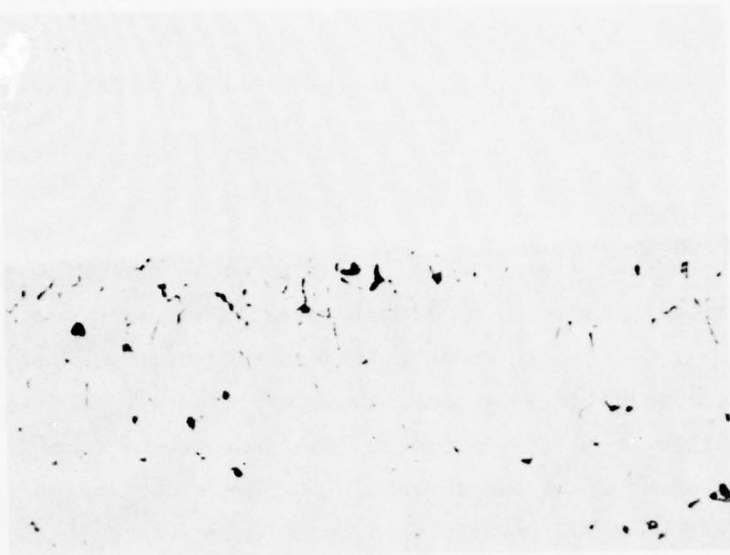
(a) Low Magnification View Showing Distribution of Bullseye Craters



500X

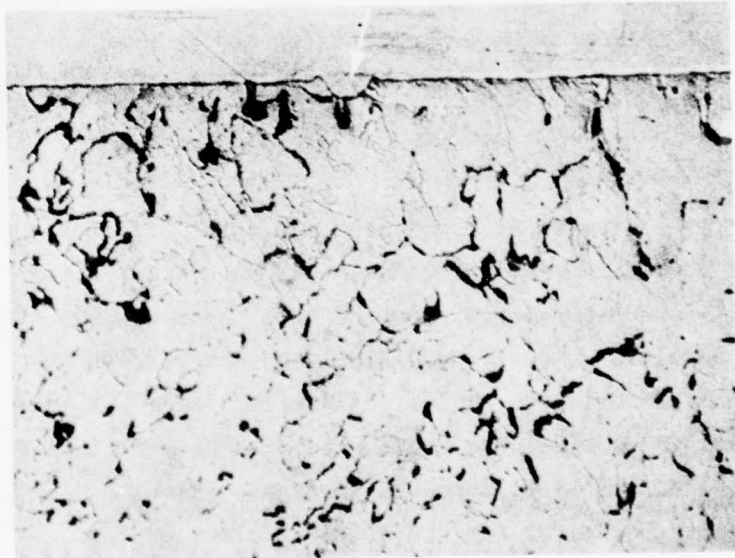
(b) High Magnification View Showing Surface Undulation and Grain Boundary Relief

FIGURE 16. VIEWS OF IRRADIATED IRON SURFACE SAMPLE F-1 (NOMARSKI LIGHTING)



800X

(a) As Polished



800X

(b) Polished and Etched

FIGURE 17. TAPER SECTIONS AT A NOMINALLY 10:1 TAPER THROUGH THE IRRADIATED SURFACE OF THE IRON SAMPLE. THE SAMPLE WAS NICKEL PLATED BEFORE SECTIONING AS INDICATED. THE ARROWS POINT TO PROFILES OF CRATERS.

the grain boundary effect just below the surface is caused by melting or a thermally induced grain boundary precipitate.

#### Pure Nickel Results

Data from nickel irradiations provided some unexpected results. The first nickel sample to be irradiated exhibited no anomalous reflectivity transient, but did appear to be melted on the surface. A second sample irradiated at somewhat higher peak power densities exhibited a stable reflectivity transient as noted in Figure 18. These transients were for the third and fourth pulse above the threshold for the effect which was found to be  $4.4 \times 10^8 \text{ W/cm}^2$  or 50% greater than the aluminum threshold. This is surprising because nickel was expected to damage at lower peak power densities than those for aluminum. No surface luminosity was observed in these irradiations.

Both samples were examined before and after irradiation at 500X with Nomarski lighting. Before irradiation, the surfaces were practically featureless which is characteristic of polished nickel. After irradiation relief of grain boundaries and surface undulation was noted. Surface undulation was greater for the sample irradiated at higher peak power densities.

#### Pure Titanium Results

Pure titanium also exhibited somewhat different behavior in the reflectivity transient measurements. A reflectivity cutoff effect was observed for peak-power density above  $2 \times 10^8 \text{ W/cm}^2$ . This effect was different from that observed in copper and aluminum, however, in that the reflectivity did not recover during the pulse and the fall time was observed to be extremely short. In essence, the surface behaved as a fast self-acting optical switch. The effect is illustrated in Figure 19 which shows the original oscilloscope records for four successive pulses on Sample T-1, one below the threshold for the effect, and three at nearly the same peak power density above the threshold. The shortest fall time is observed in Figure 19(d) and appears to be less than 5 ns. As noted in the figure, there is no curing effect as observed with aluminum and copper. Bright luminosity was observed on the surface in each instance of cutoff, but there was no indication of a

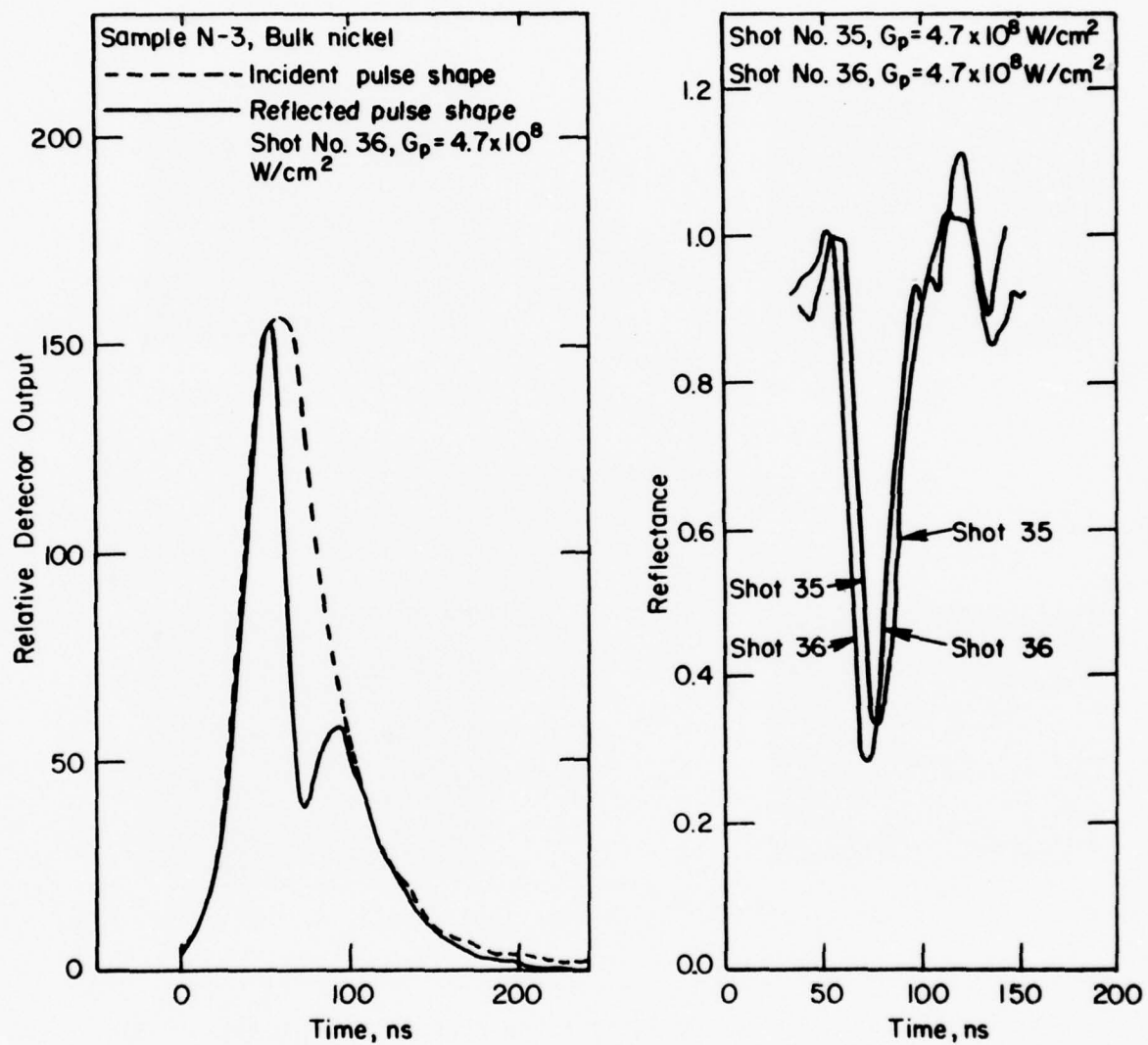
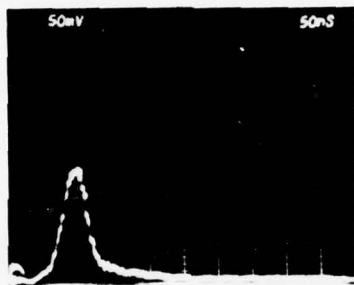
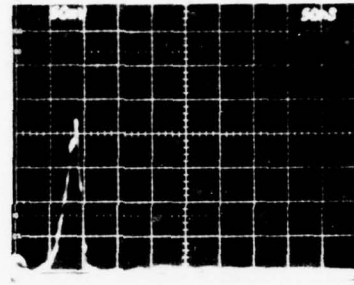


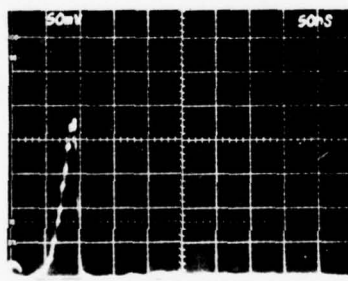
FIGURE 18. SPECULAR REFLECTIVITY TRANSIENTS FOR BULK NICKEL SAMPLE N-3



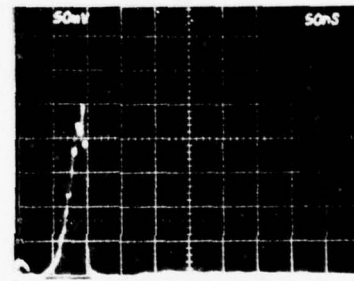
(a) Shot No. 10,  $G_p = 1.8 \times 10^8 \text{ W/cm}^2$



(b) Shot No. 11,  $G_p = 2.4 \times 10^8 \text{ W/cm}^2$



(c) Shot No. 12,  $G_p = 2.3 \times 10^8 \text{ W/cm}^2$



(d) Shot No. 13,  $G_p = 2.4 \times 10^8 \text{ W/cm}^2$

FIGURE 19. OSCILLOSCOPE RECORDS FOR BULK TITANIUM SAMPLE (T-1)  
SHOWING SHARP CUTOFF OF REFLECTIVITY WITHOUT RECOVERY

vapor plume extending from the surface as seen in aluminum film irradiations. Microscopic examination of the surfaces of Sample T-1 revealed relief of grain boundaries, but limited indication of melting.

#### Aluminum Alloy (Al 2024) Results

Three aluminum alloy samples were irradiated using conditioning sequences similar to those used for pure aluminum, only for the alloys lower peak-power densities were used. Reflectivity transients for Sample AA20-1 are presented in Figure 20(a). The first pulse to show a deviation from unity reflection was Shot No. 25 at  $1.8 \times 10^8$  W/cm<sup>2</sup> which exhibited a minimum of 75% reflectivity. On the next pulse ( $2.1 \times 10^8$  W/cm<sup>2</sup>) the reflectivity dropped to a very low value, but did not exhibit complete cutoff as occurred with pure aluminum. There was a "curing" effect, however, as is illustrated by Shot No. 28 in the figure which was typical of three pulses taken at  $2.1 \times 10^8$  W/cm<sup>2</sup> following Shot No. 26. Very faint surface luminosity was observed for Shot No. 26, but none was observed on succeeding pulses. The fact that the alloy sample was larger than optimum may have prevented observation of complete cutoff, i.e. complete cutoff may have occurred on a portion of the sample.

Sample AA20-2 was subjected to a similar sequence of pulses, but higher levels of peak power density were achieved. Incomplete cutoff of reflectivity followed by curing to a stable anomalous reflectivity effect was observed at three successive levels of peak power density (1.9, 2.1, and  $2.4 \times 10^8$  W/cm<sup>2</sup>). Following this sequence, a low-intensity irradiation was taken to check the pulse shape and then a single irradiation at each of these three levels was performed for the stabilized surface. Reflectivity transients for these irradiations are presented in Figure 20(b). As the peak power density was increased, the minimum reflectivity decreased and the duration of the "valley" portion of the transient increased. The initial drop in reflectivity was observed to be sharper for these results than in the case of pure aluminum. Incomplete recovery of reflectivity during the pulse is noted. One additional pulse at  $2.7 \times 10^8$  W/cm<sup>2</sup> was incident on the surface prior to examination of the sample. Increasing intensity of surface luminosity was observed in the latter sequence of pulses.

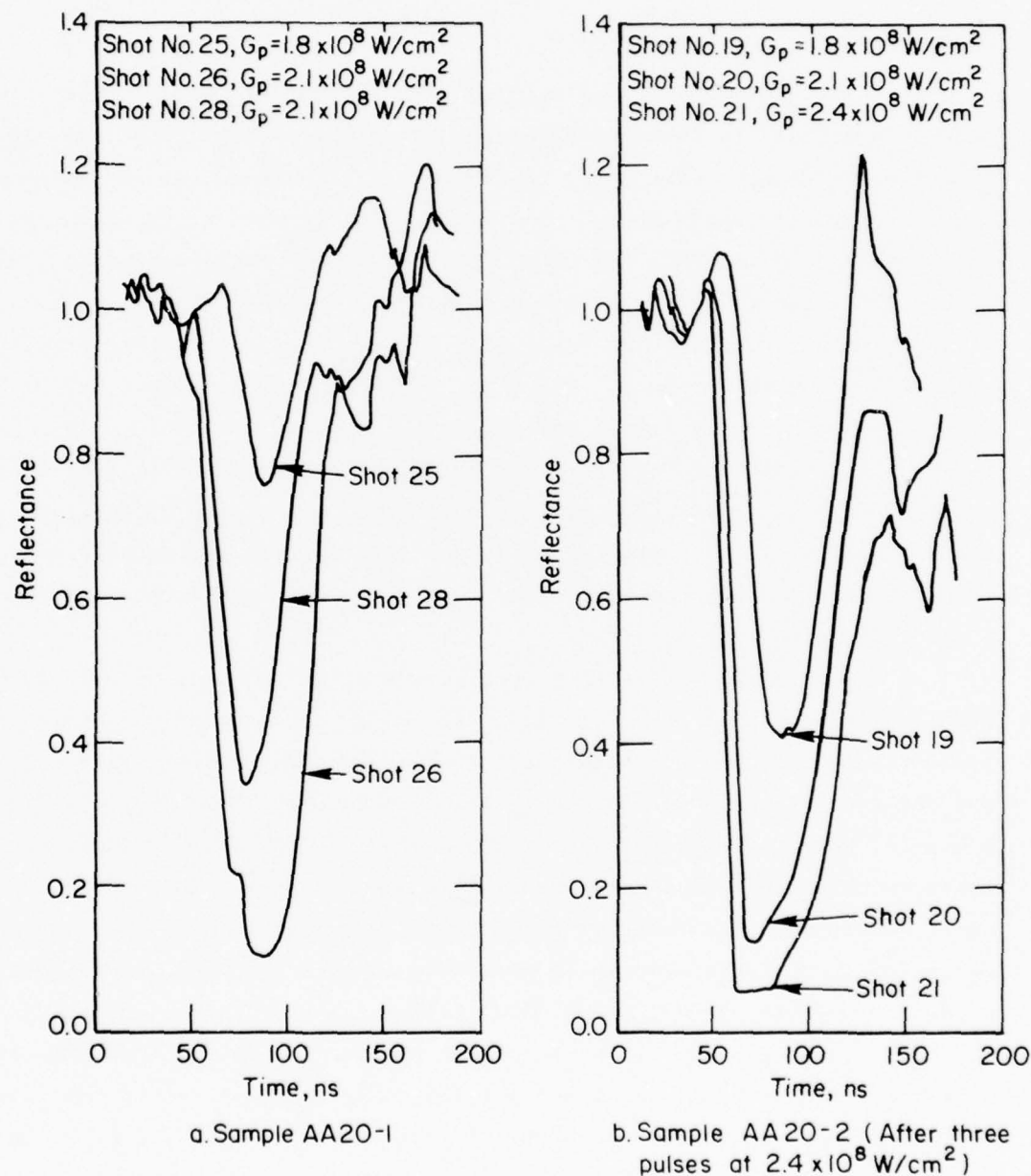


FIGURE 20. SPECULAR REFLECTIVITY TRANSIENTS FOR BULK ALUMINUM ALLOYS (2024) SAMPLES AA20-1 AND AA20-2

Sample AA20-3 was exposed to maximum beam intensities which were intermediate between those used for AA20-1 and AA20-2. Similar results were obtained and a stable anomalous reflectivity effect was observed on four successive pulses at  $2.3 \times 10^8 \text{ W/cm}^2$  peak power density.

The three 2024 aluminum samples were examined microscopically after irradiation. Nomarski micrographs were recorded at 500X for each sample before and after irradiation. The appearance of the irradiated surfaces is shown in Figure 21 in the succession of increasing irradiation intensity from Figure 21(a) to Figure 21(c) at low magnification. In addition, taper sections at a nominal 10:1 taper were made through the irradiated surface of each sample (intersection with surface is vertical in Figure 21).

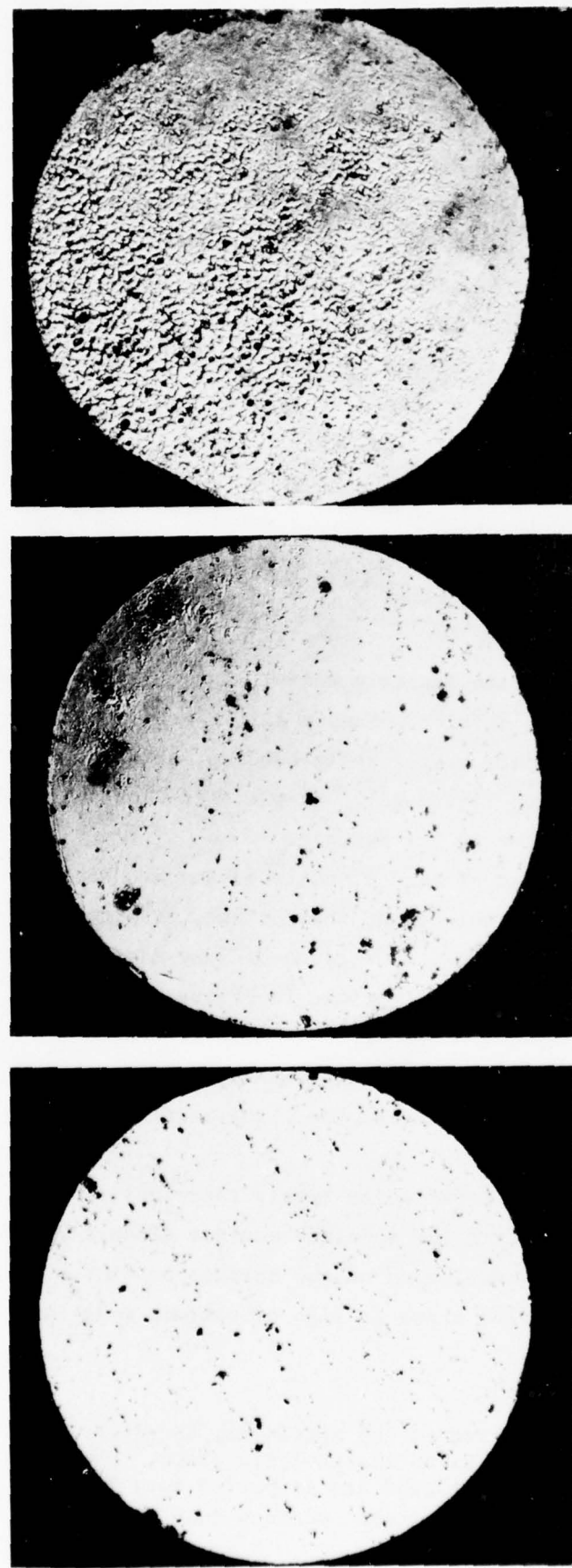
In Figure 21 minor damage is observed on Sample AA20-1 and AA20-3 ( $G_p < 2.3 \times 10^8 \text{ W/cm}^2$ ) and extensive melt is observed on Sample AA20-2 ( $G_p = 2.7 \times 10^8 \text{ W/cm}^2$ ). At 500X, Sample AA20-1 exhibited melting and vaporization of inclusions, grain boundary relief, but little surface undulation characteristic of alloy melting. Sample AA20-3 exhibited vaporization of inclusions, grain boundary relief, slip banding, and limited local undulation of the surface (see Figure 22). Sample AA20-2 exhibited bullseye craters and heavy undulation of the surface.

A taper section of AA20-1, polished and etched, is shown in Figure 23. There is no sign of melting at the surface. The taper section is nominally at a 10:1 ratio so that a distance of 1- $\mu\text{m}$  depth below the surface would appear at 10  $\mu\text{m}$  below the surface in Figure 23. At 500X, this 1- $\mu\text{m}$  distance would appear as a distance of 5 mm in Figure 23. No melting of this magnitude was seen in either Sample AA20-1 or in Sample AA20-3 which was given a higher level of irradiation. The surface sections were similar for both samples.

At the highest irradiation level, there was substantial interaction of the laser beam with the specimen surface (Figure 21(c)). The taper section shows both the undulation on the surface and the section through the surface (Figure 24(a)), but shows no sign of surface melt layer\*. However,

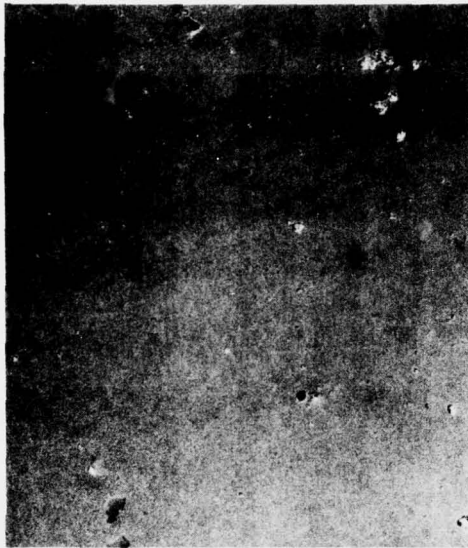
---

\* Because of the small size of the specimens, an electroless nickel plate had to be used instead of an electrolytic plate. The adherence of the electroless plate was not good and it pulled away from the surface in Figure 24 exposing the irradiated surface (out of focus).



35X  
(a) Sample AA20-1, Maximum Peak Power Density,  $2.1 \times 10^8 \text{ W/cm}^2$   
(b) Sample AA20-3, Maximum Peak Power Density,  $2.3 \times 10^8 \text{ W/cm}^2$   
(c) Sample AA20-2, Maximum Peak Power Density,  $2.7 \times 10^8 \text{ W/cm}^2$

FIGURE 21. LOW MAGNIFICATION VIEWS OF IRRADIATED SURFACES OF THE 2024 ALUMINUM ALLOY SAMPLES (NOMARSKI LIGHTING)



500X

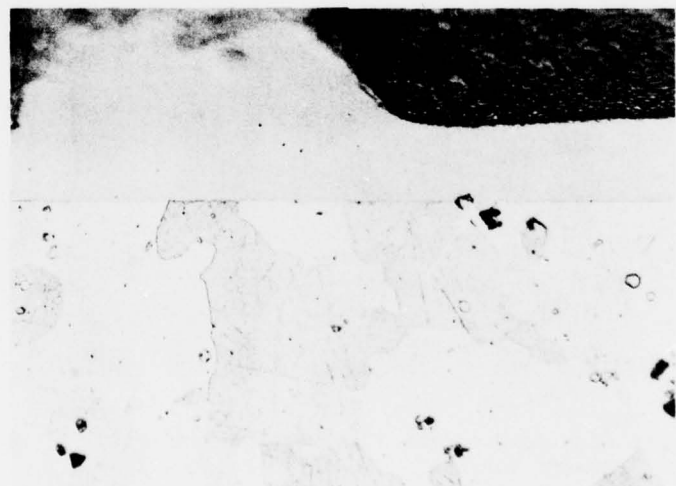
(a) Before Irradiation



500X

(b) After Irradiation

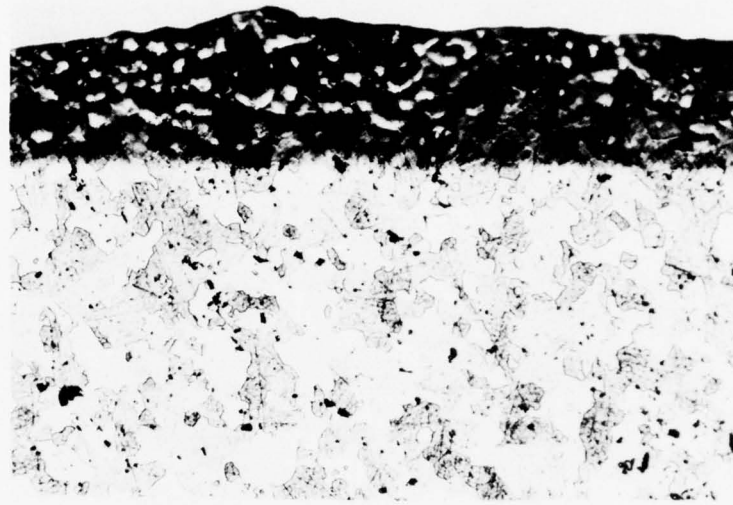
FIGURE 22. NOMARSKI MICROGRAPHS OF SAME AREA OF SURFACE OF SAMPLE AA20-3 (SUBJECTED TO  $2.3 \times 10^8 \text{ W/cm}^2$ )



6J385

500X

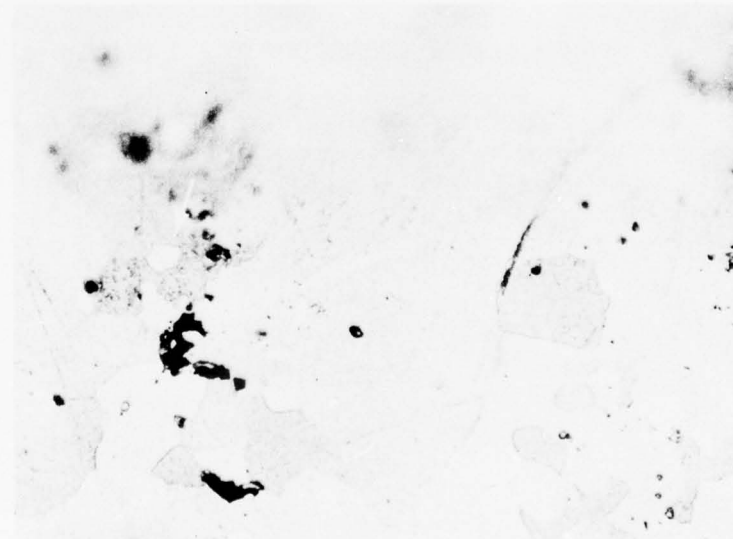
FIGURE 23. TAPER SECTION AT 10:1 THROUGH THE IRRADIATED SURFACE OF SAMPLE AA20-1. ARROW INDICATES BLOWN OUT INCLUSION.



6J387

100X

(a) View Showing Both the Original Irradiated Surface (Dark Region) and the Taper Section



6J389

500X

(b) The Edge Between the Taper Section and the Irradiated Surface. The Arrow Points to a Serrated Grain Boundary on the Original Irradiated Surface.

FIGURE 24. TAPER SECTION OF THE SAMPLE SUBJECTED TO THE HIGHEST BEAM INTENSITY (AA20-2)

on the etched irradiated portion of the surface which can be seen directly in Figure 24(a), many of the grain boundaries show tiny serrations as shown by the arrow in Figure 24(b). This would indicate that there has been some grain boundary migration which might have resulted from melting of a very thin film followed by epitaxial regrowth. Alternatively, this serration might result from rapid grain boundary migration near the melting temperature. If this limited melt occurred, it is expected it would have to be much less than  $1\text{-}\mu\text{m}$  deep to have shown no in-depth indication of melting, such as a preferred orientation of the grain boundaries near the surface or change in etching response. This result may be consistent with the extremely short duration of the pulse and resultant rapid quenching. Longer pulse durations will produce a clearly defined melt zone in aluminum alloys. In another program, 7075 aluminum alloy surface was irradiated with a normal TEA laser pulse with nitrogen in the laser (400-ns pulse width). A well-defined melt layer approximately  $10\text{-}\mu\text{m}$  thick was observed after irradiation in that case.

#### Titanium Alloy (Ti-6-4) Results

A titanium alloy sample was subjected to a series of irradiations of increasing peak power density. An anomalous reflectivity transient was first observed at  $1.5 \times 10^8 \text{ W/cm}^2$ . This transient is displayed in Figure 25. A drop to 50% reflectivity followed by incomplete recovery is noted. Upon increase of the intensity to  $1.7 \times 10^8 \text{ W/cm}^2$ , the minimum reflectivity dropped to 5% as noted in the figure. Subsequent irradiations at the same intensity produced complete cutoff of reflectivity followed by slight recovery during the pulse. A pulse at  $2.2 \times 10^8 \text{ W/cm}^2$  caused complete cutoff with no recovery during the pulse. In essence the titanium alloy results were very similar to those for pure titanium, except that the threshold for the effect was slightly lower for the alloy and the rate of fall of the reflectivity was not as great.

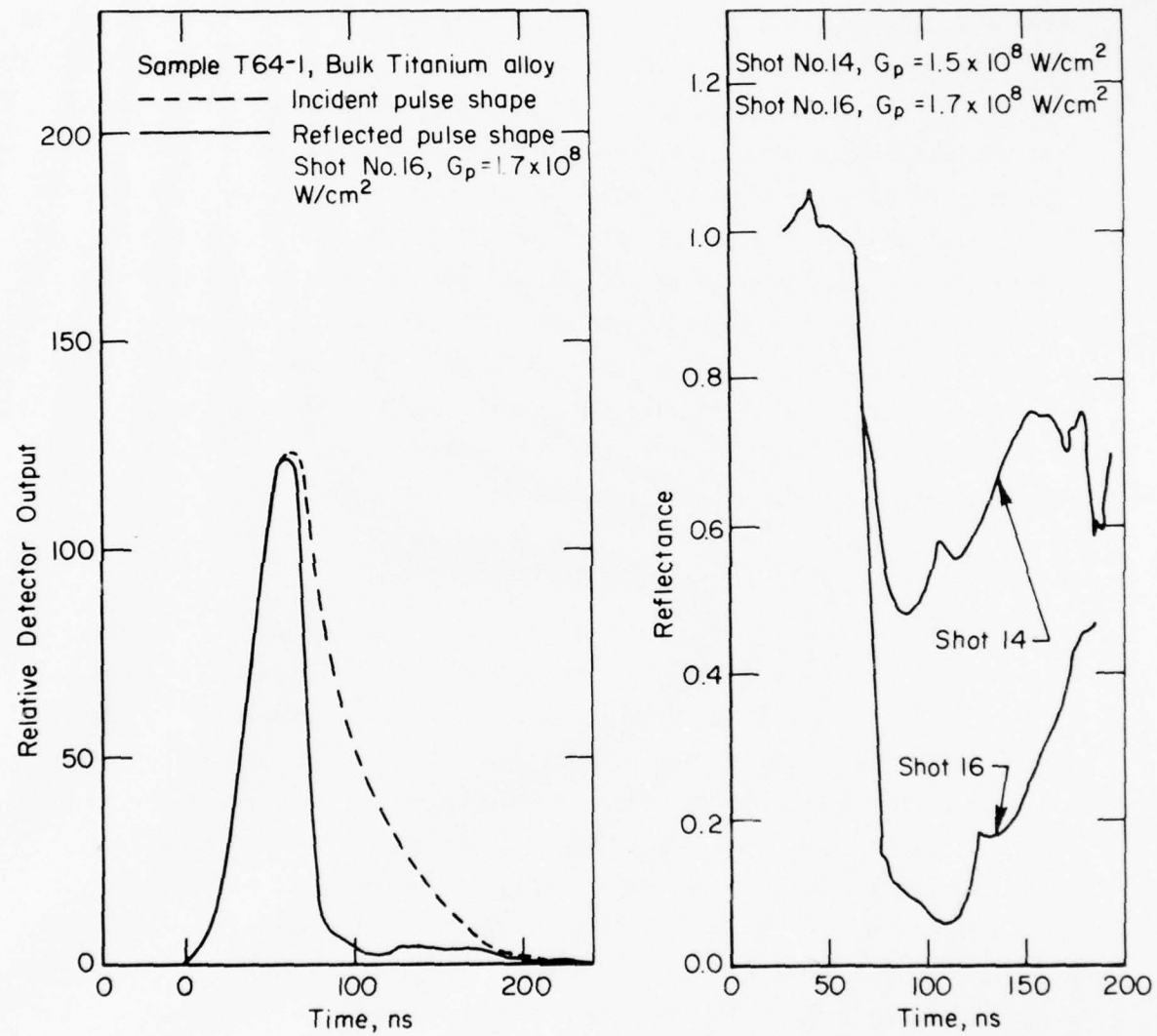


FIGURE 25. SPECULAR REFLECTIVITY TRANSIENT FOR BULK TITANIUM ALLOY (Ti-6-4) SAMPLE T64-1

DISCUSSION OF RESULTS

It is clear from the preceding section that a new effect has been observed in the specular reflectivity behavior of metals and alloys subjected to intense pulses of  $10.6\text{-}\mu\text{m}$  radiation in vacuum. Anomalous decreases in specular reflectivity to levels typically less than 40% of the initial value followed by complete recovery during the laser pulse have been observed. The effects are reproducible and highly material-dependent in their detail. In this section, the important experimental results are summarized, heat-transfer predictions are discussed, and implications for the LSD-wave initiation problem and materials processing applications are addressed.

Summary of Experimental Observations

The anomalous reflectivity effect observed consisted typically of a very sharp drop in specular reflectivity midway in the laser pulse to a minimum value lying in the 5-40% range followed by nearly complete recovery to the initial reflectivity late in the pulse. The duration of the deviation from unity reflectivity was in the 30-80-ns range.

The general shape of the reflectivity transient was similar for most materials with duration and minimum value being dependent upon laser beam peak-power density and material. No repeatable structure on the transients was observed which could be definitely related to the plateau effects observed at  $1.06\text{-}\mu\text{m}$ .<sup>(5,8)</sup> The thresholds for the stable anomalous reflectivity effect for the various materials studied are presented in Table 2. Some materials are noted to behave similarly in some of the details of the anomalous reflectivity effect.

The soft materials, aluminum and copper (and to some extent the 2024 aluminum alloy), exhibit a complete cutoff in specular reflectivity with recovery during the laser pulse for irradiations above a fixed threshold intensity. The cutoff effect is always "cured" on a succeeding pulse at the same intensity, i.e. either no deviation from unity will occur or a stable non-zero transient will be observed. Cutoff will again occur for each first pulse at a higher intensity with curing following. The effect appears to be triggered by impurities, voids, or inclusions which act as absorption centers.

TABLE 2. SUMMARY OF ANOMALOUS REFLECTIVITY BEHAVIOR IN METALS AND ALLOYS

<u>Material</u>	<u>Stable Anomalous Reflectivity Effect Threshold (10<sup>8</sup> W/cm<sup>2</sup>)</u>	<u>Cutoff Effect</u>	<u>Recovery from Cutoff During Pulse</u>		<u>Curing Effect</u>	<u>Light Emission</u>	<u>Slip Banding</u>	<u>Bullseye Craters</u>
Aluminum	3.5	yes	yes		yes	faint <sup>(a)</sup>	yes	yes
Copper	>5.4	yes	yes		yes	faint	yes	yes
Iron	1.6-2.0	no	--	--	--	no	no	yes
Nickel	4.4	no	--	--	--	no	no	a few
Titanium	1.8-2.4	yes	no		no	strong	no	no
Al 2024	1.8	incomplete	yes		yes	yes	yes	yes
Ti-6-4	1.5	yes	no		no	strong	no	no

(a) Very faint compared to the brilliant plume created by vaporization of 120-nm layer of aluminum at  $0.6 \times 10^8$  W/cm<sup>2</sup>.

There is apparently a range of thresholds for these absorption centers which are purged from the surface at different intensities. It is not believed that absorption in metal vapor plays a role in either the cutoff effect or the anomalous reflectivity effect. Only weak surface luminosity is observed which is uncharacteristic of the bright plume which would be expected for vaporization of even a thin 100-nm layer of aluminum.

Except for thresholds, the reflectivity behavior of nickel and iron was very similar. The anomalous reflectivity effect was observed, but no cutoff effect occurred. No surface luminosity was observed confirming that metal vapor absorption is not a necessary factor in the anomalous reflectivity effect.

Pure titanium (and to some extent the titanium alloy Ti-6-4) behaved somewhat differently than all of the above materials. A sharp cutoff effect was observed which was not "cured" by repeated pulsing. In the case of pure titanium the reflectivity dropped from unity to zero in a time interval less than 5 ns. No recovery of reflectivity during the pulse was observed, except in the case of the alloy. Bright surface luminosity observed with open-shutter photography indicated that vaporization may have occurred for these samples.

Generally, the microscopic examination of samples indicated surface alteration in cases where the anomalous reflectivity effect was observed. Surface relief observed in Nomarski micrographs was indicative of melt in the case of pure aluminum and examination of a taper section confirmed a  $1\text{-}\mu\text{m}$  melt layer for one multiple-pulsed aluminum sample. The aluminum alloy, however, exhibited the anomalous reflectivity effect and little evidence of melt (other than inclusions) in the surface appearance or microstructure as seen in taper section. The absence of definitive evidence may be a result of the short laser pulse employed.

#### Comparison of Experimental Data With Theoretical Predictions

To support the interpretation of the experimental results, theoretical predictions of the thermal response of samples subjected to laser pulses were performed. Heat-transfer calculations were performed with an explicit finite-difference computer code, TRAHT 2, which solves the transient heat

conduction equation in two dimensions for multiregion geometries with a wide variety of boundary conditions. For correlation of the current experimental results, one-dimensional calculations for aluminum were performed. The model for absorptivity of the laser radiation was based upon the work of Wieting and Schriempf<sup>(19)</sup> who employed a Drude-Lorentz model having a temperature-dependence determined from d.c. conductivity data. The results of their calculations are approximated in Figure 26 by the solid line. The dashed line is simply a linear extrapolation from the value of absorptivity just above the melt point,  $T_m$ . The behavior of absorptivity in the melt is not well understood, but the linear dependence should provide an upper limit if the temperature dependence is determined by d.c. conductivity variation alone. The absorptivity above the vaporization point,  $T_v$ , was assumed to be 1.0.

Results of surface temperature calculations for a 100-nm-thick aluminum thin film are presented in Figure 27 for a narrow range of peak power densities near threshold for melt. The dashed lines present results for the case of an insulated thin film while the solid lines show results at the same intensities for a calculation including the effect of conduction into the quartz substrate. Even though the quartz has a relatively low thermal conductivity, the thermal conduction during the pulse is obviously significant. If the film behaved as modeled, the solid curves of Figure 27 indicate that the quartz could quench the melted film for peak power densities as much as 20% greater than the melt threshold,  $2.3 \times 10^7$  W/cm<sup>2</sup>. The experimental results tend to indicate that this may not be the case. The early portion of the heating curve (and hence the threshold for melt) are probably modeled quite well. If the thermal contact with the substrate is reduced by film lift-off during the pulse, the heating rate would rise more sharply as indicated by the insulated film temperature histories. This would explain the observed binary nature of the film damage. Whether or not the film lifts off, however, the model predicts structure in the reflectivity transients as noted in Figure 28, which presents calculated reflectivity transients for the temperature histories of Figure 27. Predicted structure in the transient associated with the melt transition was not observed in the thin-film experiments. The experimental data are more consistent with either a much sharper rise in absorptivity with temperature above

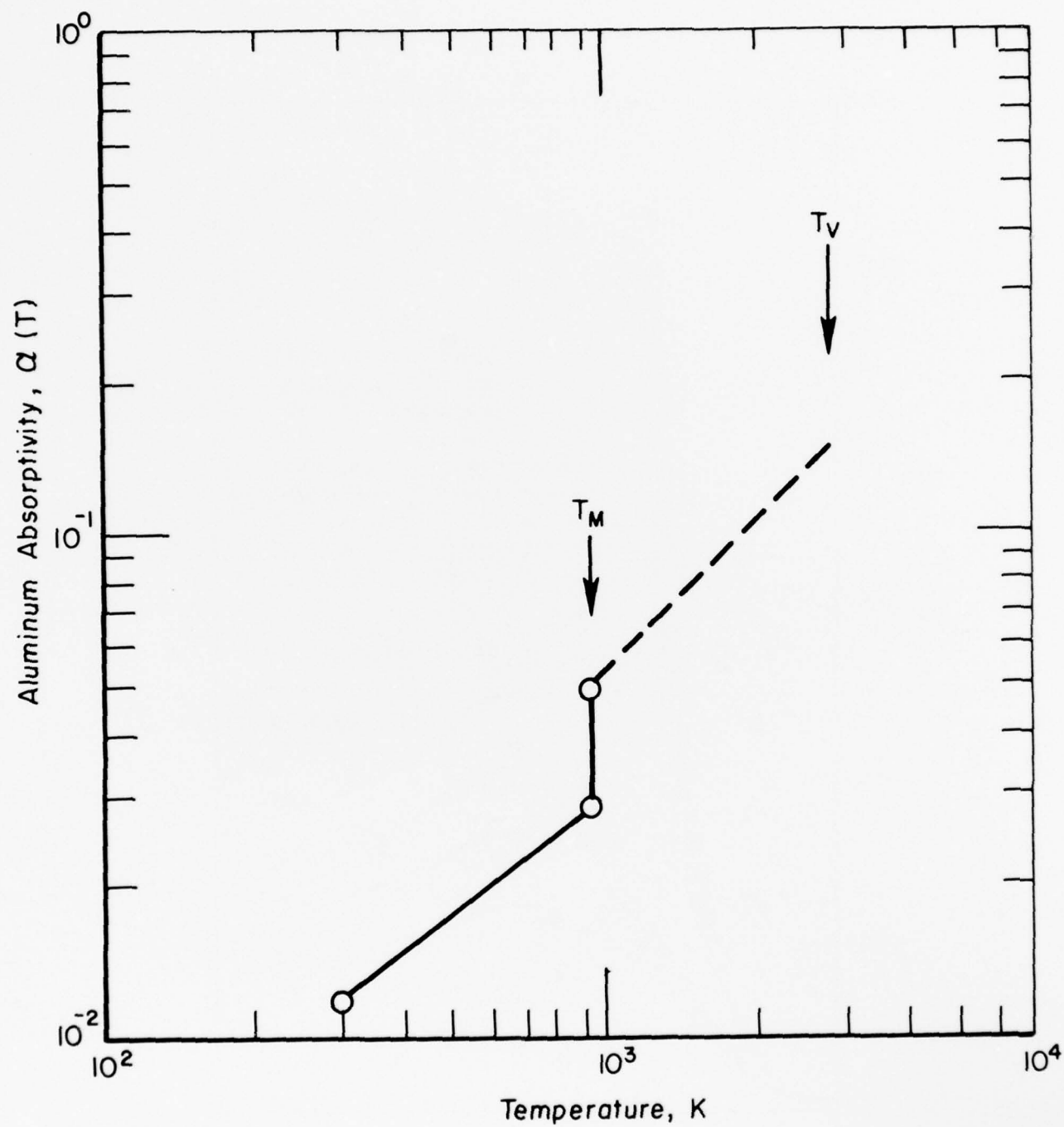


FIGURE 26. PURE ALUMINUM ABSORPTIVITY MODEL AT  $10.6 \mu\text{m}$  WAVELENGTH

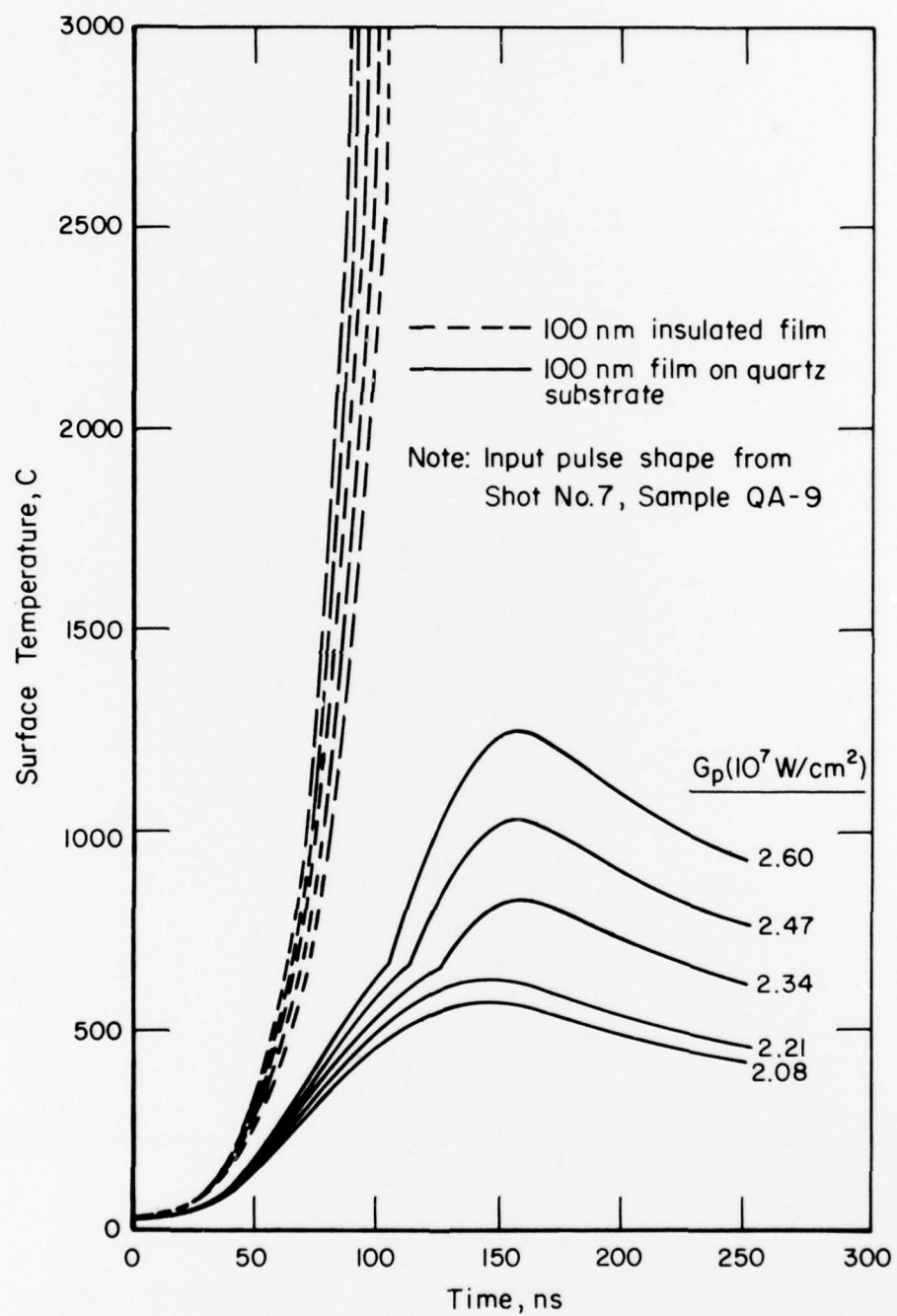


FIGURE 27. PREDICTED SURFACE TEMPERATURE HISTORY FOR ALUMINUM THIN FILM

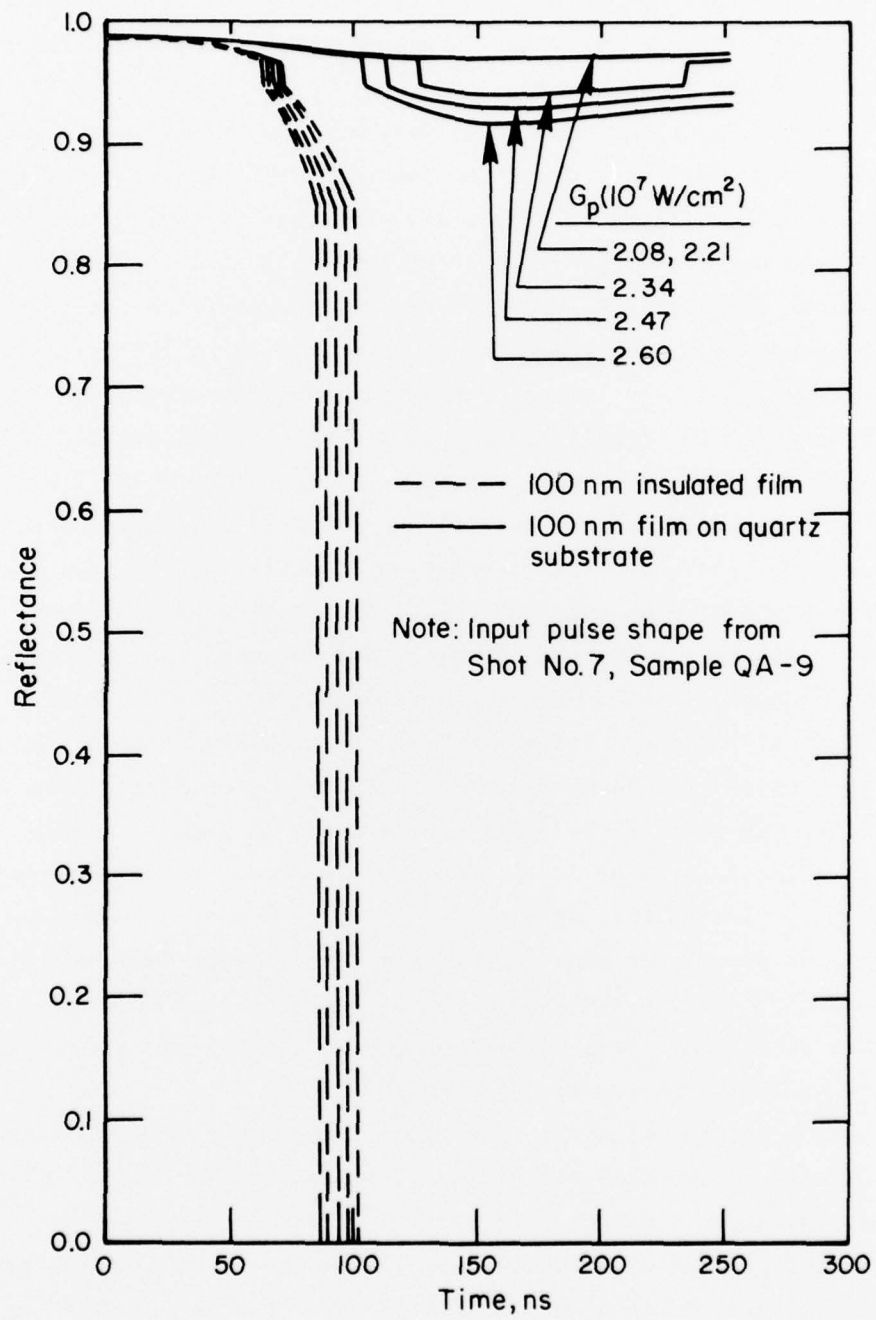


FIGURE 28. PREDICTED REFLECTIVITY TRANSIENT FOR ALUMINUM THIN FILM

the melt point than assumed in the model or a transition to a transparent (dielectric-like) state in the film at the melt point and associated direct absorption in the quartz substrate.

Surface temperature histories were also calculated for the bulk aluminum sample at peak power densities near the melt threshold for this case. Results are presented in Figure 29. The melt threshold for bulk aluminum is seen to be near  $3.1 \times 10^8 \text{ W/cm}^2$  which is in reasonable agreement with damage observations. For two of the transients the melt is predicted to be quenched during the pulse. The predicted reflectivity transients resulting from these temperature histories are presented in Figure 30. Comparison of these transients with those which were measured indicates a considerable disagreement with the model. It is noted in the figure that the predicted time interval from initial drop in reflectivity to recovery (resolidification) increased dramatically with increasing peak power density. A much weaker dependence of this interval on intensity was observed experimentally. The greatest disparity, however, was the magnitude of the measured reflectivity minimum compared with that predicted, 0.2-0.4 vs. 0.85. If it is assumed that all incident energy is either specularly reflected or absorbed in a thin surface layer (assumptions of the model), then it is clear from the curves of Figure 29 that if the reflectivity drops to values of order 0.4 when the surface melts (instead of dropping to 0.9 as predicted), then the surface temperature will rise to the vaporization point in a matter of several nanoseconds even for peak power densities only slightly above threshold for melt. In other words, the reflectivity data cannot be reconciled with the simple heat-transfer theory in a self-consistent way in the absence of surface vaporization which was not observed for aluminum.

Heat transfer calculations were not made for all metals studied, but estimates of the expected materials effects on damage threshold were made by comparing values of a damage figure of merit based on optical and thermal properties. This figure of merit is essentially the threshold peak power density for melt with a linearly rising pulse of risetime  $\Delta t$ ,

$$G_f = \frac{\Delta T_m}{\alpha_0} \left[ \frac{9\pi k\rho C_p}{16 \Delta t} \right]^{1/2}, \quad (4)$$

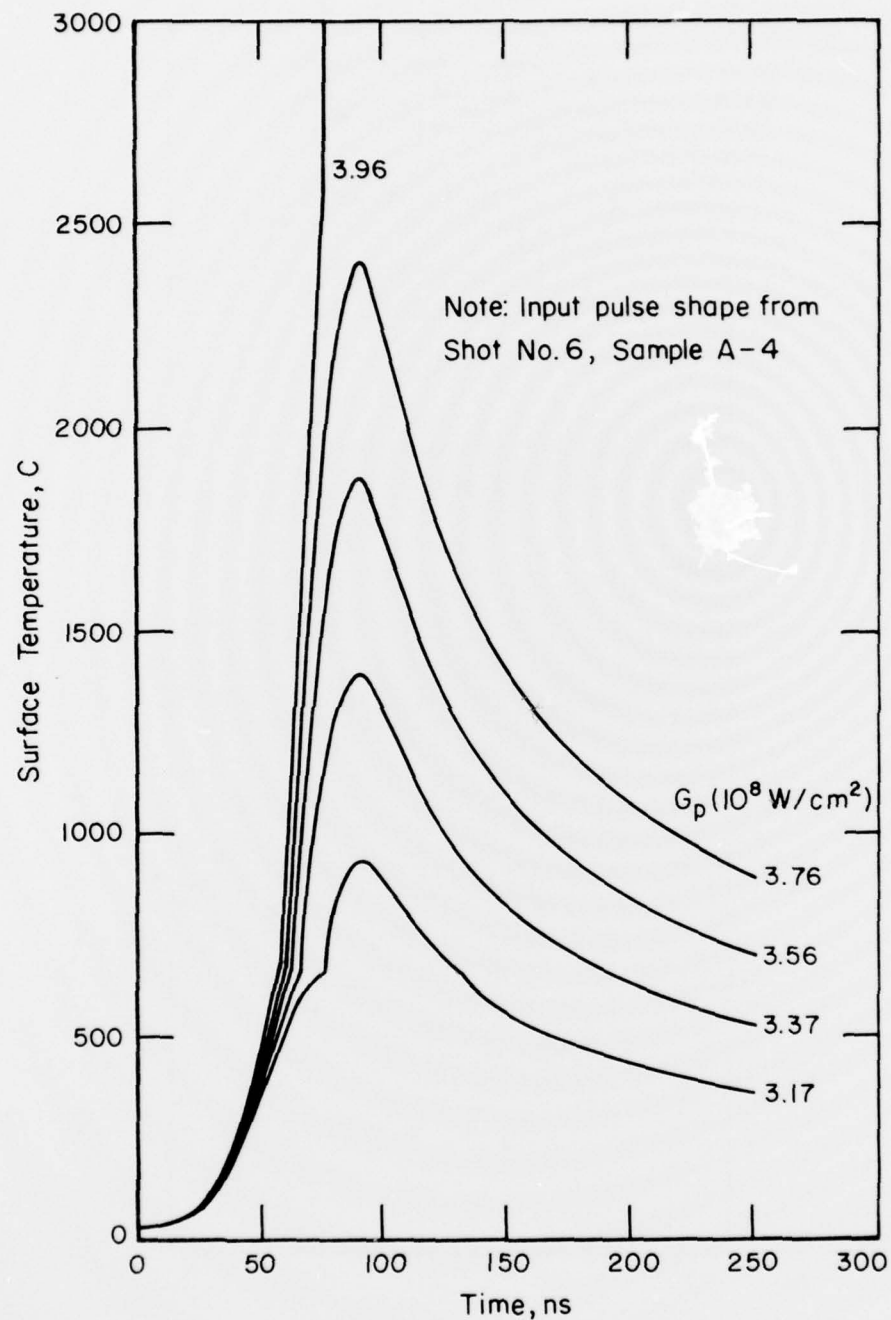


FIGURE 29. PREDICTED SURFACE TEMPERATURE HISTORY OF BULK ALUMINUM SAMPLE

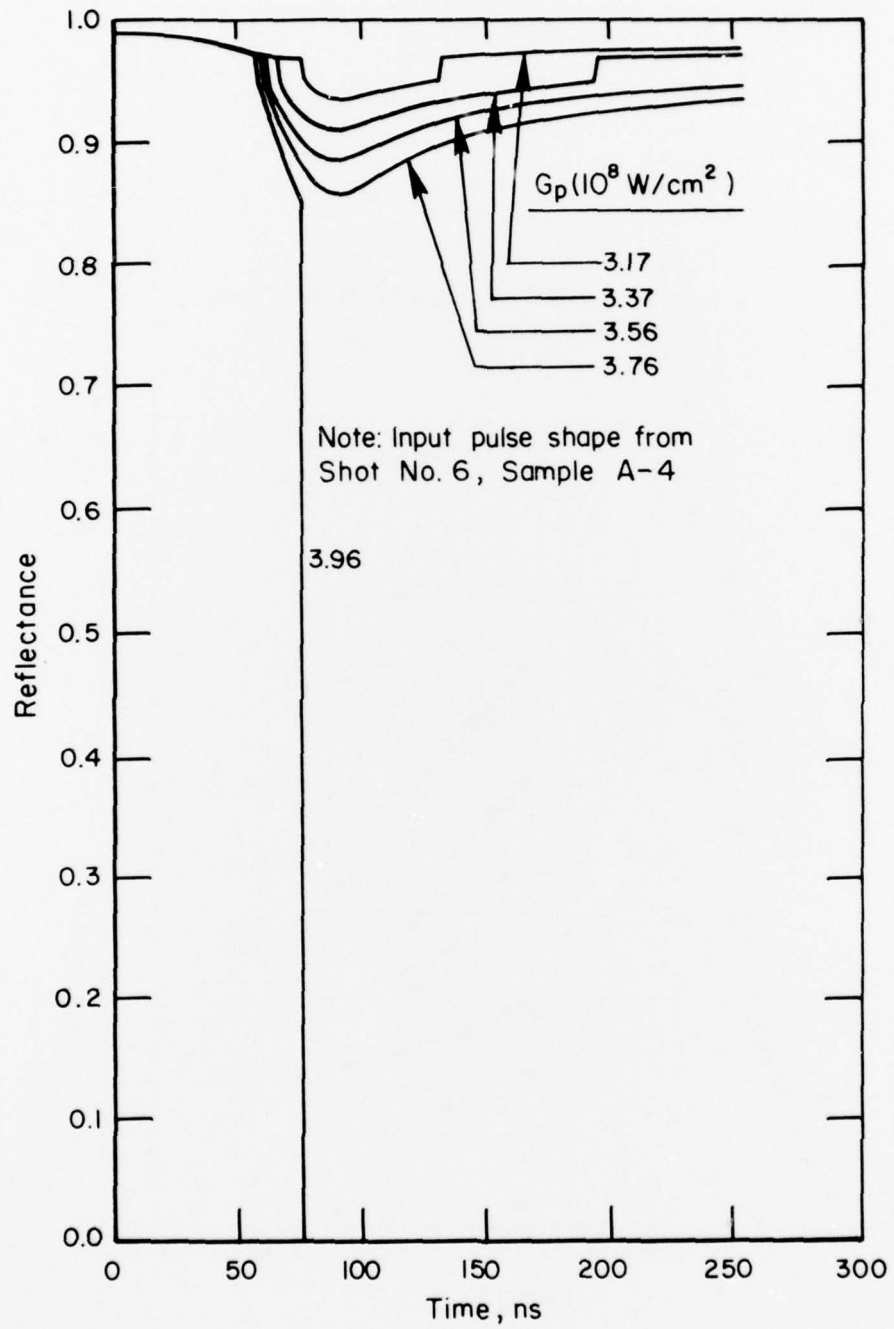


FIGURE 30. PREDICTED REFLECTIVITY TRANSIENT  
FOR BULK ALUMINUM SAMPLE

where  $\Delta T_m$  is the temperature rise to melt,  $\alpha_0$  is the room temperature absorptivity,  $k$  is thermal conductivity,  $\rho$  is density, and  $C_p$  is specific heat. Properties used to calculate values of this figure of merit for the materials studied are presented in Table 3. Figure 31 shows a graph of experimentally determined threshold values for the stable anomalous reflectivity effect as a function of corresponding predicted damage thresholds based on the simple figure of merit. It should be noted that the figure of merit overpredicts the damage threshold as indicated by comparison of the detailed heat-transfer results for aluminum ( $G_p = 3.1 \times 10^8 \text{ W/cm}^2$ ) with the aluminum figure of merit corresponding to the same room temperature absorptivity ( $G_f = 8.4 \times 10^8 \text{ W/cm}^2$ ). The discrepancy is a result of the combined effect of variation of  $\alpha$  below the melt temperature and significant deviation from linearity in the actual pulse shape. If the correction for this effect were the same for all metals, then a good correlation of the anomalous reflectivity effect with damage would be indicated in Figure 31 by proximity of all data to the dashed line drawn through the aluminum result. Only iron correlates well in addition to the aluminum. A lower bound only is shown for copper since a stabilized anomalous reflectivity effect was not observed in that case. The nickel threshold for the anomalous reflectivity effect is well above the damage threshold, as was confirmed in the experiments. The aluminum alloy, however, exhibited little damage at the effect threshold which is somewhat inconsistent with the implications of Figure 31. The titanium alloy shows the greatest discrepancy and indicates that perhaps a minimum power density is required for the anomalous reflectivity effect in addition to the melt condition. This minimum power density would be in the  $1-2 \times 10^8 \text{ W/cm}^2$  range, but additional data would be needed to confirm this aspect of the effect.

#### Implications of the Anomalous Reflectivity Result

It is clear from the previous section that a simple temperature-dependent absorptivity function cannot be extracted from the experimental reflectivity results in a self-consistent manner using only the surface-driven thermal model. If the limited experimental evidence showing no vaporization (for aluminum, nickel, and iron) is accepted, then the apparent high surface absorption leads to contradictory thermal predictions. Hence, it is important to reexamine the possible options for the ultimate fate of the beam energy and possible

TABLE 3. PROPERTY DATA USED IN CALCULATION OF  
DAMAGE THRESHOLD FIGURE OF MERIT

<u>Material</u>	<u>Room Temperature Absorptivity, <math>\alpha_0</math></u>	<u>Temperature Rise to Melt, <math>\Delta T_m</math> (C)</u>	<u>Density<sub>3</sub> (gm/cm<sup>3</sup>)</u>	<u>Specific Heat <math>C_p</math> (J/cm C)</u>	<u>Thermal Conductivity <math>k_0</math> (W/cm C)</u>	<u>Threshold Figure of Merit, <math>G_f</math> (10<sup>8</sup> W/cm<sup>2</sup>)</u>
Aluminum	0.012~0.02	633	2.70	0.90	2.35	5.0~8.4
Copper	0.007~0.012	1056	8.93	0.39	4.01	22~38
Iron	0.06	1509	7.86	0.45	0.83	2.9
Nickel	0.032~0.059	1426	8.80	0.44	0.94	3.0~5.7
Titanium	0.03~0.09	1643	4.50	0.52	0.22	0.87~2.6
Al 2024	0.053	611	2.77	0.84	1.20	1.3
Ti-6~4	0.13	1620	4.47	0.54	0.074	0.36

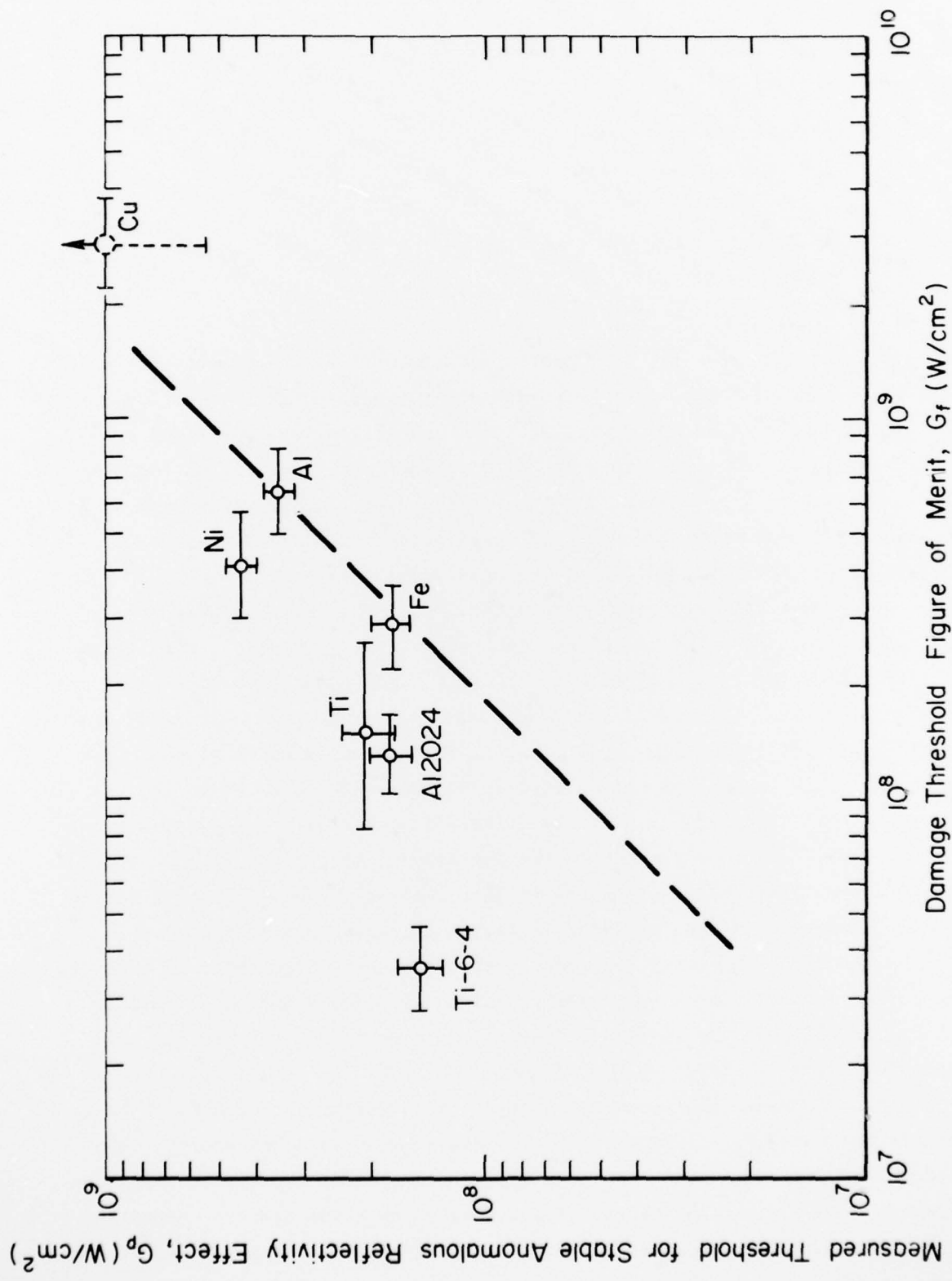


FIGURE 31. CORRELATION OF EXPERIMENTAL THRESHOLD DATA WITH PREDICTED DAMAGE THRESHOLDS

origins of the anomaly. It is believed that the energy partitioning is among the following:

- Specular reflection
- Diffuse reflection
- Vaporization
- Electron emission
- Reradiation
- Substrate conduction.

As noted before, it is not likely that diffuse reflection can account for all of the anomaly because of the extremely rapid recovery of specular reflectivity observed during the pulse, i.e. a heavily rippled surface would not be expected to recover to a specular surface, particularly on the time scale observed. Vaporization also is not believed to carry away much of the beam energy, based on the absence of a characteristic luminous plume for irradiations exhibiting the anomalous reflectivity effect.

The remaining processes are believed to be the ones most likely to account for the anomaly. It has been suggested by Musal<sup>(20)</sup> that thermal decoupling of the electrons from the lattice might occur at beam intensities above  $10^8 \text{ W/cm}^2$ . This would certainly lead to surface electron emission which could carry off some of the energy. Intense surface emission of radiation might be expected under such conditions, but none was observed in the visible region of the spectrum. A slightly different mechanism was suggested by Karas et al.<sup>(21)</sup> to explain electron emission timing. They propose that the electron distribution function is distorted in the presence of a strong source (laser radiation) and sink (emission current) in momentum space, which leads to high-energy electrons. The fact that large emission currents do indeed occur has been confirmed experimentally for aluminum at  $10.6 \mu\text{m}$  in vacuum,<sup>(22)</sup> but the magnitude of the total energy emitted was not comparable to that incident on the surface.

The remaining process, substrate conduction, is believed to be a viable mechanism for dissipation of the anomalously absorbed energy, even though the simple thermal model employed in this study contradicts this contention. In the simple theory, it was assumed that the optical absorption depth was much less than the thermal penetration depth corresponding to the

shortest characteristic time of interest (for  $\Delta t = 10^{-10}$  s,  $\Delta x = [\kappa \Delta t]^{1/2} \approx 10^{-5}$  cm) and the laser heating was treated as a surface flux. While this assumption holds for low-temperature absorptivities, it may not hold under conditions of anomalous absorption. In particular, optical penetration of 1.06  $\mu\text{m}$  radiation through a 30- $\mu\text{m}$  layer of mercury (without vaporization) has been observed under intense irradiation.<sup>(13)</sup> This metal-to-dielectric transition has also been observed for aluminum by detection of ultraviolet radiation transmitted through a 17- $\mu\text{m}$  foil.<sup>(23)</sup> If optical penetration of this magnitude occurs for 10.6  $\mu\text{m}$ , the heating of the metal would be distributed over a greater volume and the maximum volumetric heating rate would drop during the anomaly by two orders of magnitude. This would prevent surface temperatures from reaching the vaporization point while still permitting dissipation of the increased laser energy absorbed. The recovery of reflectivity observed during the pulse may simply be an indication of quenching of the dielectric state.

While the detailed mechanisms operative have not been isolated, the experimental results of this program confirm that the early heating processes in LSD-wave initiation on metals does entail anomalously high absorption as postulated in earlier work.<sup>(1)</sup> In addition, a possible alternate source of priming electrons for initiating the LSD-wave plasma has been identified. If the electron distribution function is altered in the course of the anomalous reflectivity transient, an enhanced thermionic emission of electrons might be expected. An additional implication of the results relates to the use of pulsed lasers in processing of metals by surface heating. If the ultimate fate of the anomalously absorbed energy is conduction to the substrate, then an increase in effective coupling coefficient can be realized using pulses. In addition, by careful control of the pulse length, it should be possible to use the initial portion of the pulse to create an absorbing surface and the remaining portion of the pulse to efficiently add energy to produce a melt layer of controlled thickness. Accurate prediction of the temperatures and quench-rates will require measurements to improve our understanding of the spatial distribution of the deposition of laser energy in addition to the temporal data acquired in this program.

CONCLUSIONS AND RECOMMENDATIONS

Conclusions which may be drawn from the research reported herein are;

- An anomalous effect has been observed in the specular reflectivity of smooth aluminum surfaces subjected to intense  $10.6 \mu\text{m}$  pulses. The effect on stabilized surfaces is reproducible and consists of a very sharp drop in specular reflectivity midway in the pulse to a minimum value lying in the 5-40% range followed by nearly complete recovery to the initial reflectivity late in the pulse. The duration of the deviation from unity reflectivity was in the 30-80 ns range.
- The threshold for the effect in aluminum correlates well with the predicted and observed melt thresholds.
- A special variant of the effect exists for aluminum (and copper) wherein complete cutoff of reflectivity occurs on a first shot at levels well above the melt threshold. This cutoff effect is apparently triggered by surface impurities and is "cured" on a subsequent pulse at the same intensity.
- The anomalous reflectivity effect occurs generally in several other pure metals (copper, iron, nickel, titanium) and two alloys (Al 2024, Ti-6-4); however, the details of the behavior varies strongly with material and alloying.
- The measured thresholds for the effect indicate a general trend related to the melt threshold provided that a minimum peak power density is exceeded ( $\approx 10^8 \text{ W/cm}^2$ ).
- A pure titanium surface subjected to intensities above threshold for the effect behaves as a fast, self-acting optical switch, i.e. cutoff of reflectivity with no recovery during the pulse. The effect does not cure on subsequent pulses; to the contrary, the fall time was found to decrease to less than 5 ns.
- Vaporization plays no essential role in the anomalous reflectivity effect for aluminum, iron, and nickel.

- If the nonreflected energy is absorbed on the surface, simple heat-transfer theory leads to contradictions with observed results. The theory can be reconciled with the experiment, however, if optical penetration is allowed (as might occur with a metal-to-dielectric transition).
- The most likely partitioning of the nonspecularly reflected energy is among electron emission, reradiation, and substrate conduction. The latter appears to be most consistent with existing data.

Based on these conclusions and results of the program in general, it is clear that certain additional measurements are in order to clarify details of this new effect. It is, therefore, recommended that future investigations of the anomalous reflectivity effect be directed along the following lines of investigation:

- Determine energy partitioning by measurement of coupling coefficient, vuv radiation intensity, electron emission current, ion emission current, vapor flux, and diffuse reflectance.
- Determine the importance of melting in triggering the effect by measurement of reflectivity transients with samples preheated to various temperatures below melt.
- Determine the role of metal-to-dielectric transitions and associated optical penetration by measurement of foil transmission during irradiation.
- Determine experimentally the effect of pulse shape and length on the thermal patterns achieved as evidenced by melt layer thickness and uniformity.

REFERENCES

- (1) C. T. Walters, R. H. Barnes, and R. E. Beverly III, *J. Appl. Phys.* 49, 2937 (1978).
- (2) C. T. Walters, *Appl. Phys. Lett.* 25, 696 (1974).
- (3) R. E. Beverly III and C. T. Walters, *J. Appl. Phys.* 47, 3485 (1976).
- (4) D. A. Reilly (private communication).
- (5) A. M. Bonch-Bruevich, Ya. A. Imas, G. S. Romanov, M. N. Libenson, and L. N. Mal'tsev, *Soviet Phys.-Tech. Phys.* 13, 640 (1968).
- (6) M. K. Chun and K. Rose, *J. Appl. Phys.* 41, 614 (1970).
- (7) G. R. Levinson and V. I. Smilga, *Sov. J. Quant. Electron.* 4, 680 (1974).
- (8) T. E. Zavecz, M. A. Saifi, and M. Notis, *Appl. Phys. Lett.* 26, 165 (1975).
- (9) V. A. Batanov, F. V. Bunkin, A. M. Prokhorov, and V. B. Fedorov, *Sov. Phys. JETP* 36, 311 (1973).
- (10) R. V. Karapetyan and A. A. Samokhin, *Sov. J. Quant. Electron.* 4, 1141 (1975).
- (11) F. B. Bunkin, *Sov. J. Quant. Electron.* 4, 1143 (1975).
- (12) S. I. Anisimov, A. M. Bonch-Bruevich, M. A. El'yashevich, Ya. A. Imas, N. A. Pavlenko, and G. S. Romanov, *Sov. Phys.-Tech. Phys.* 11, 945 (1967).
- (13) A. M. Bonch-Bruevich and S. E. Potapov, *Soviet Tech. Phys. Lett.* 1, 167 (1975).
- (14) J. C. Koo and R. E. Slusher, *Appl. Phys. Lett.* 28, 614 (1976).
- (15) J. F. Ready, *IEEE J. Quant. Electron.* QE-12, 137 (1976).
- (16) C. T. Walters and A. H. Clauer (to be published in *Appl. Phys. Lett.*)
- (17) D. L. Decker, J. M. Bennett, M. J. Soileau, J. O. Porteus, and H. E. Bennett, *Opt. Eng.* 17, 160 (1978).
- (18) J. O. Porteus, M. J. Soileau, and C. W. Fountain, *Appl. Phys. Lett.* 29, 156 (1976).
- (19) T. J. Wieting and J. T. Schriempf, "Free-Electron Theory and Laser Interactions with Metals", Report of NRL Progress, Naval Research Laboratory, Washington, D.C., June, 1972 (unpublished).
- (20) H. M. Musal (private communication).
- (21) V. I. Karas, S. S. Moiseev, and V. E. Novikov, *JETP Lett.* 21, 245 (1975).

(22) C. T. Walters, R. H. Barnes, and R. E. Beverly III, "An Investigation of Mechanisms of Initiation of Laser-Supported Absorption (LSA) Waves", Semianual Report, January, 1975, Contract No. DAAH01-73-C-0776, Battelle Columbus Laboratories.

(23) Yu. I. Dymshits, Sov. Tech. Phys. Lett. 2, 294 (1976).